Experimental Study and Geometrical Method to Design Bio-inspired Robotic Kinematic Chains of Inching-Locomotion Caterpillars

José Cornejo[1], J. Enrique Sierra-Garcia[1], Francisco Javier Gomez-Gil[1], Juan Grados[2], Ricardo Palomares[3], Alfredo Weitzenfeld[4]

[1]Department of Electromechanical Engineering, University of Burgos, 09006 Burgos, Spain.
[2]Departamento de Entomología, Museo de Historia Natural de la Universidad Nacional Mayor de San Marcos. (UNMSM), Av. Arenales 1256, Jesús María, Lima, 15072, Peru.
[3]Professional School of Mechatronics Engineering, Universidad Ricardo Palma, Lima, Peru.
[4]Biorobotics Laboratory, Department of Computer Science and Engineering, University of South Florida, Tampa, FL, USA.

∗ Corresponding author.
E-mail address: jose.cornejo@ieee.org (J. Cornejo).

Abstract

Inching-locomotion caterpillars (ILAR) show impressive environmental adaptation, having high dexterity and flexibility. To design robots that mimic these abilities, a novel Bioinspired Robotic Design (BIROD) method is presented. The method is composed by an algorithm for Geometrical Kinematic Analysis (GEKINS) to standardize the proportional dimensions according to the insect's anatomy and obtain the kinematic chains. The approach is experimentally applied to analyze the locomotion and kinematic chain of these specimens: *Geometridae* – 2 pair of prolegs (represents 35,000 species) and *Plusiinae* – 3 pair of prolegs (represents 400 species). The obtained data indicate that the application of the proposed method permits to locate the attachment mechanisms, joints, links, and to calculate angular displacement, angular average velocity, number of degrees of freedom, and thus the kinematic chain. *Geometridae* in contrast to *Plusiinae*, shows a longer Walk-Stride Length (WSL), a lower number of single-rotational joints in 2-D (3 DOF versus 4 DOF), and a lower number of dual-rotational joints in 3-D (6 DOF versus 8 DOF). The application of BIROD and GEKINS provides the forward kinematics for 35,400 ILAR species and are expected to be useful as a preliminary phase for the design of bio-inspired arthropod robots.

Keywords: biomimetic, bio-inspired robot, engineering design, robot kinematics, inching-locomotion caterpillar, arthropod animals

1. Introduction

Many insect species show impressive environmental adaptive locomotion due to their technical features of morphology and evolved biomechanics for inching, climbing, crawling, swimming, rolling, and walking on various complex surfaces [1-6]. This has inspired the development of various bio-inspired robots that imitate certain physical as well as behavioral attributes [7-9]. For example, during the past years, bio-inspired crawling and climbing robots have been developed for various applications like maintenance, surveillance, and cleaning. Thus, researchers have succeeded in creating robots focusing on the bio-symbiosis concept [10, 11] to enlarge their workspace and improve its flexibility and adaptability [12-14]. This concept has been applied to robotic mechanisms like wheels, legs, propellers, etc., with flexible multi-links and innovative adhesion pads based on the bio-symbiosis concept, using rigid and compliant actuation components [15, 16].

To improve the manipulability and mobility of robotic systems, the Worcester Polytechnic Institute (WPI) [17] performed an analysis on insect/animal species that have inspired the design of mechatronic systems [18]. The aim was to select the best option for designing the morphology of future robots. The study consisted of a comparison based on: mobility, manipulability, ease of control, mechanism simplicity, cost and power consumption, where the following robots were considered: a) Mobile robot with four bar links, b) Wall Climbing Robot, c) Flying Drone, d) Quadrupedal Robot, e) Inch Worm. Regarding the resulting data, the ILAR showed promising locomotion behavior, high flexibility, as well as mechanism simplicity. These results are encouraging indicators of high flexibility over surfaces or structures, moreover, its morphology provides high control dexterity for moving at any location and orientation.

Since the 1990s [19], caterpillars have been inspiring the application in the robotics field integrating kinematic chains [20, 21]. The larvae of 2 main groups of species of

Lepidoptera caterpillars, *Geometridae* - Taxonomic Hierarchy: Family (that has 35,000 species – 2 pairs of prolegs "C-2PP") [22-26] and *Plusiinae* - Taxonomic Hierarchy: Subfamily (that has 400 species – 3 pairs of prolegs "C-3PP") [27-32] can be found in many places around the world. To our knowledge, only 2 robotics projects worked on locomotion analysis and kinematic chain design of *Geometridae* (called "Inch-worm") [33-35]. The locomotion of a novel specie, *Plusiinae*, which is similar to *Geometridae*, has not been analyzed previously, and although is similar to *Geometridae*, it has some morphological-technical different characteristics that also mark a great potential to be used in robotics. Moreover, to the best of our knowledge, no previous paper standardizes the proportional dimensions of kinematic chains for inching-locomotion caterpillars.

A number of robot designs inspired by caterpillar locomotion have been developed from 1990 [36] up to the present day [37, 38]. A preliminary search was performed with respect to DOF, locomotion capability, and locomotion surface, as these are considered the main parameters observed in animal/insect walk-stride [39-42]. It is noted that in these designs, with median DOF is 5, most are capable of horizontal and vertical displacement on flat surfaces.

This work proposes to study the inching-locomotion of two main groups of species of Lepidoptera caterpillars in order to use those kinematic chains for future works applying to the design of bio-inspired robots or mechatronic machines with the ability to perform tasks with high dexterity and flexibility and taking into consideration the features of reconfigurability and modularity. To this aim, a new algorithm is proposed for the experimental study of ILAR. Moreover, a comparative analysis is performed between the two species, *Geometridae*, and *Plusiinae*, taking into account: a) kinematic models and WSL, b) joint locations, c) D-H parameters, d) joint angle's behavior – covering angular displacement (θ) and angular average velocity (ω), e) DOF in 2-D and 3-D.

The remainder of the manuscript is organized as follows. In Section 2, materials and methods are described, and we introduce the BIROD methods and GEKINS algorithm for bio-inspired robot design of inching-locomotion caterpillars. In Section 3, the results are shown focusing on the biomechanical locomotion analysis of kinematic chains in 2-D and 3-D, where joint angular's displacement and velocity are described. In Section 4, the discussion is presented following comparisons with former similar robots. The paper ends with the conclusion and future works.

2. Materials and Methods

2.1. Materials

2.1.1. Biological Material

To perform this study, third-instar larvae of 2 species of Lepidoptera were used. All of them were maintained in the laboratory under high-quality environmental conditions, with temperature (18 – 22°C) and humidity (70 - 90%) [43]:

a) *Geometridae* (represented by Sabulodes sp.) – 20 caterpillars, obtained from 2 colonies located in La Molina, Lima (Peru, 12.0820° S, 76.9282° W) and Chosica, Lima (Peru, 12.0097° S, 76.9054° W). One subject was selected with a sample average MYL dimension (Taken it from between A5-A6 segments to T2 segment): 22 ± 0.2 mm, which can be rounded to 22 mm.
b) *Plusiinae* (represented by Triclopusia, sp.) – 20 caterpillars, obtained from 2 colonies located in Cercado de Lima, Lima (Peru, 12.0464° S, 77.0428° W) and Chorrillos, Lima (Peru, 12.1849° S, 77.0075° W). One subject was selected with a sample average MYL dimension (Taken it from between A5-A6 segments to T2 segment): 20 ± 0.4 mm, which can be rounded to 20 mm.

The two species that were collected, caterpillars of Sabulodes sp. (*Geometridae*) and Trichoplusia sp. (*Plusiinae*), are described in the next paragraphs focusing on the functional morphological part, which is directly related to the objective of our work. The larvae of Lepidoptera are elongated and cylindrical, it consists of three parts: head, thorax and abdomen. The head is a rounded and sclerotized capsule, where the mouthparts (mandibles, maxillae, and labium) and sensory organs such as antennae (chemoreceptors) and stemmata (single-lens visual organs) are located. In the inner part of the head, there are modified salivary glands, which produce silk, made of proteins, and used for aerial dispersal and shelter building. The thorax is made up of three segments, each of which has a pair of legs, which are made up of the following parts: coxa, trochanter, femur, tibia, tarsus, and claw. The abdomen is made up of 10 segments; most prolegs between the third and sixth segments and, in the tenth segment (anal prolegs). These prolegs, which are paired ventral muscled outgrowths of the body wall are used for locomotion. Between the segments of the thorax and abdomen, an intersegmental membrane allows elongation and contraction movements [44-47].

a. Sabulodes sp. (*Geometridae*)

Represents the C-2PP. The morphology of the observed specimens of the *Geometridae*, as can be shown in Figure 1, presents three thoracic segments (T1, T2, T3), each one with a pair of legs, and ten abdominal segments. Prolegs are present at the sixth (A6) and tenth (A10) abdominal segments prolegs) [22]. For kinematic chain design purposes, the Main Body Length (MYL) means the summation of segment lengths from A8 to T2.

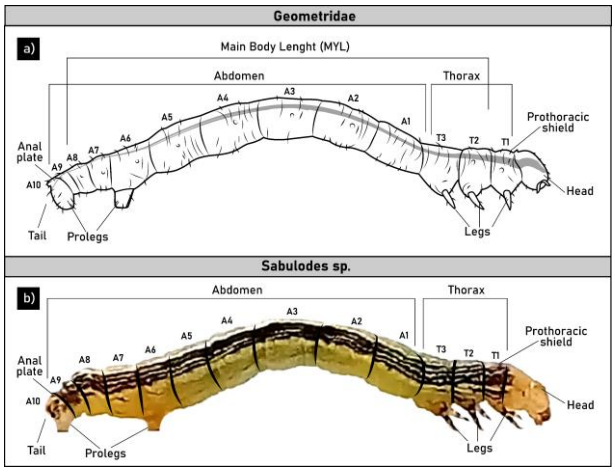

Figure 1. a) *Geometridae* Morphology, b) Sabulodes sp.

The locomotion of *Geometridae sp*. describes a long stride (Appendix 1 – Figure A.1.):

Long stride: fixed on the surface through the prolegs at A6 and A10, the caterpillar stretches the thoracic segments and part of the abdomen. When it finds a safe place to hold on to, it does so with the thoracic leg claws, immediately retracting the rest of the body and placing A6 prolegs very close to T3, forming a dorsal hump with the rest of the body. Then, held with A6 and A10 prolegs, it stretches the thorax and part of the abdomen to search for the next holding point.

b. Trichoplusia sp. (*Plusiinae*)

Represents the C-3PP. The morphology of the observed specimens of the *Plusiinae*, as can be shown in Figure 2, presents three thoracic segments (located at T1, T2, T3), each one with a pair of legs, and ten abdominal segments. Prolegs are present in the fifth (A5), sixth (A6), and tenth (A10) abdominal segments [27]. For kinematic chain design purposes, the Main Body Length (MYL) means the summation of segment lengths from A5 to T2.

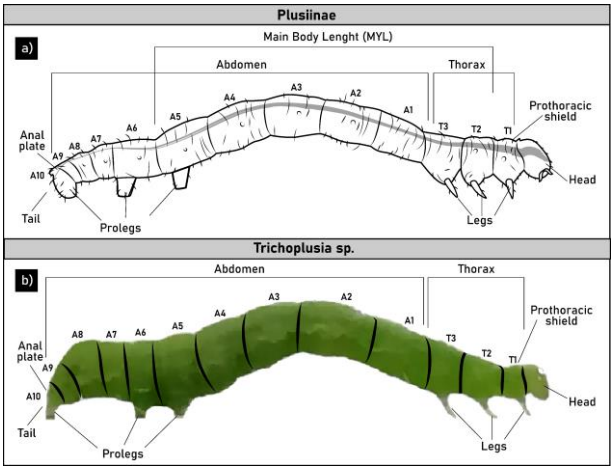

Figure 2. a) *Plusiinae* Morphology, b) Trichoplusia sp.

The locomotion of *Plusiinae sp.* describes long and short strides (Appendix 2 – Figure A.2.):

1) Long stride: Attached to the surface through the thoracic legs, it contracts A7 to A10, bringing A10 prolegs closer to A6 and fixing them to the surface. It immediately raises the A6 prolegs and then A5 ones, stretching these segments and attaching itself to the surface by A6 prolegs first, then by A5 ones. It then moves forward the abdominal and thoracic segments, attaches itself to the surface through the thoracic legs, raises A10 prolegs, then those at A6 and A5, moves forward a short space, and finally, lands A6 prolegs and then A5 ones. Once again, it rises A6 and A5 prolegs, arching the body as much as possible, forming an inverted "U" from T3 to A6, attaching its body through A6 and A10 prolegs. At this moment A5 prolegs are drawn close to T3 legs; A5 prolegs descend and at this moment the head and thorax rise over the surface; first T3 legs and then simultaneously T1 and T2 ones. Immediately the body stretches looking for support points for the thoracic legs. They attach themselves to these and can repeat the operation. Sometimes a variation is observed, where, resting on A10 prolegs, it rises A6 prolegs and then those at A5, then contracting the body and dragging A10 prolegs in a single movement.

2) Short stride: for this movement, holding onto the surface through the thoracic legs, it rises A10 prolegs and retracts the body, placing A10 prolegs next to A6 or as far as it decides to move. Attached to the surface with A10 prolegs, it lifts A6 prolegs first and then those at A5, to immediately stretch these two segments. After this, prolegs at A6 descend, next A5 prolegs do so too. It then immediately stretches the closest anterior segments forward and moves the thoracic legs forward.

2.1.2. Experimental platform

1. Three high-resolution cameras of POCO M4 Pro 5G (Xiaomi),
2. One container where the larva's movement is observed that measures 19 x 10 x 5.5 cm.
3. One incandescent bulb placed over the platform: 20 Watts, regulated below 1500 Lumens.

2.1.3. Hardware and software

1. Computer ASUSTeK, Processor AMD Ryzen 9 5900HX with Radeon Graphics. Video: Nvidia GEFORCE RTX. 16GB RAM. Windows 10.
2. CorelDRAW® version 2022.
3. Matlab R2022b® Software with Robotics Toolbox developed by Peter Corke [48], which was formalized/coded by the simulation based on SerialLink.

2.2. Method

This study called the BIROD method, which covers a new proposal for geometric morphometrics analysis [49] and forward kinematics, applied for ILAR, has been performed following 6 steps (Figure 3):

1. Caterpillar collection.
2. Experimental observation by video recording.
3. Choose the images from the video, selecting 8 PHAWS, and process them for scaling dimensions.
4. Apply the novel GEKINS algorithm and use D-H convention to define the mechanical parameters.
5. Biomechanical locomotion analysis in 2-D, where end-effector position and joint angle's behavior (angular - displacement / average velocity) are presented.
6. Biomechanical locomotion analysis in 3-D, for kinematic representation.

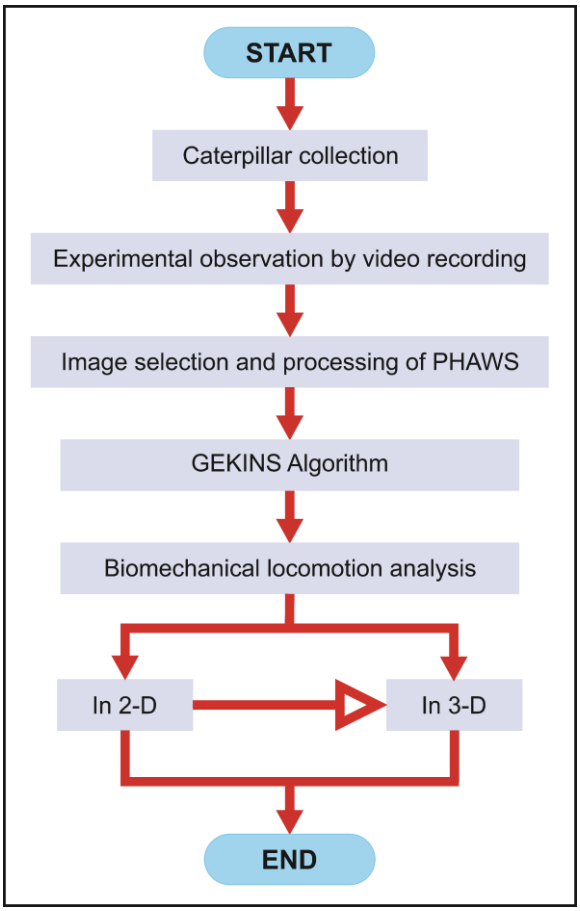

Figure 3. Workflow diagram of the BIROD method, beginning with the insect collection, until the biomechanical locomotion analysis in 2-D/3-D.

Each of them was developed using terminologies of the ISO/TC 266 standard [50], taking into account biomimetic foundations for learning from nature, such as biomimicry, biomechanics, and bionics [51-54].

2.2.1. Caterpillar collection

This method was tested on 2 specimens of Lepidoptera [43]: a) *Geometridae* (represented by *Sabulodes sp.)* – 20 caterpillars, b) *Plusiinae* (represented by *Triclopusia, sp.*) – 20 caterpillars. As described in section 2.2.1., all of them were maintained in the laboratory under good environmental conditions, also they were intact and healthy during the experiments, where 2 subjects were selected (1 by each species) due to their average MYL.

2.2.2. Experimental observation by video recording

During the experiments, up to 5 larvae were placed in the starting end of the container, and they were left there for one minute to adapt to the new environment. During the observation break between new specimens, the floor of the container was cleaned with water to remove any physical or chemical evidence of previous occupants. The experiments were conducted at night, the most active circadian phase for rhythmic feeding and locomotion [55]. This measuring equipment was emplaced indoors where temperature (18 – 22°C) and humidity (70 - 90%) are early stable.

A high-resolution video recording system was used for locomotion observation (tracking system) of caterpillars, essentially made up of a motion capture module, which has 3 cameras, placed on 2 locations for frontal view, and 1 for top view. It records at a speed of 60 fps with a resolution of 1920 x 1080 pixels (50 MP). The visual field of the camera is about 19 x 10 cm. Providing that the image resolution of the camera: 1920 x 1080 pixels, the real-world resolution is approximately 10 pixels/mm, which is enough to reach satisfying results (Figure 4). Lighting was controlled with 1 incandescent bulb placed over the platform: 20 Watts, regulated below 1500 Lumens, to reduce injuries to the specimens. The light was turned off periodically during the photographic sessions to avoid the habituation of the larva.

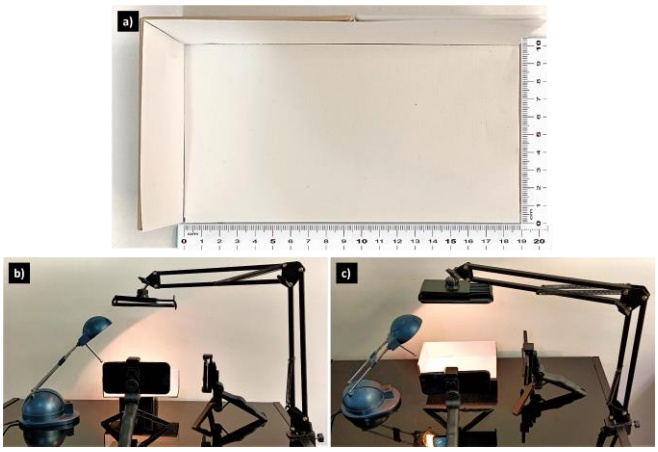

Figure 4. Observational Platform. a) Dimensions, b) Lateral Video Capture, c) Top Video Capture.

2.2.3. Image selection and processing of PHAWS

After taking the videos, the image processing was developed using CorelDRAW® (Other software could be used, such as: Adobe Illustrator, Photoshop, etc.). For scaling dimensions at 1:100, select t_0-t_7 PHAWS, which are the photograms that show different states of the insect. To get a specific location in 2-D space, a coordinate grid composed of the X and Y axis is placed above t_0 to t_7, where each square measures 100 mm x 100 mm (Appendix 1 – Figure A.1. and Figure A.2.). Note that due to the kinematic chain's length in real life could change (From S_1 to S_2), in order to compare both insects, we consider re-scaling the real dimension to an adjusted length, so the new dimension is 24 mm (it implies that is a multiple of 8, where L is an integer number).

Criteria to select the photograms of caterpillar's PHAWS (Appendix 1):

1. t_0 - maximum length's body amplitude/starting walk-stride.
2. t_4 - minimum length's body amplitude/body completely shrank.
3. Divide the time elapsed between t_0-t_4, in 5 equal states, where the t_1, t_2 and t_3 can be taken.
4. t_5 - head up.
5. Divide the time elapsed between t_5-t_7, in 2 equal states, where the t_6 can be taken.
6. t_7 – almost maximum length's body amplitude/finishing walk-stride.

2.2.4. GEKINS algorithm and D-H Convention

The novel GEKINS algorithm proposed in the BIROD method is stated by inputs and outputs, also the kinematic modeling process of the caterpillars is divided into 6 steps, as shown in Appendix 2 - Table A). Note that, the caterpillar's anatomy is flexible and can been modelled following the flexible robotics paradigm; however, the complexity of sensing and controlling flexible joints limits its applicability in practice, thus the current design analysis follows a multi–rigid body system approach. The aim is to obtain a model that will allow the construction of physical robots using rigid materials that can be accurately and robustly controlled. Considering the aforementioned features, the robot's motion will not have the flexibility of the living creature, but following bio-inspiration behavior principles [56, 57], we can recreate a similar walk-stride. In addition, the kinematic chains are designed to be represented by a serial manipulator called articulated robot based on rotational joints.

As shown in Figure 5, at the left are located the instructions for C-2PP, while at the right for C-3PP, and at the center the information that fits for both. Then process from step 1 to step 4 is validated for 2-D modeling, then adding step 5, the 3-D kinematics are able to be defined. In addition, the outputs are used to perform the biomechanical locomotion analysis. Then. according to Figure 5, in order to locate each component of the Kinematic Chain: Before starting with Step 1 of GEKINS, the t_0 phase was selected due to its maximum length – "B" (for *Geometridae*, 22 mm and for *Plusiinae* 20 mm, between S_1 and S_2) because during its locomotion the body works emulating an accordion. Note that *Geometridae* has 2 pairs of prolegs (C-2PP) guided by data shown in Figure 1, and *Plusiinae* has 3 pairs of prolegs (C-3PP) based on the information presented in Figure 2. In addition, the process of kinematic modeling is explained in the following steps (Appendix 1 – Figure A.1. and Figure A.2.). Note that the GEKINS starts on the t_0 phase, which means that first, Steps 1 to 5 are applied on the t_0 phase, then the method is reproduced from t_1 to t_7.

STEP 1:

Attachment Mechanisms - in this case, the Suction Cups *(S)* localization:

- For C-2PP, S_1 between 2 prolegs (in the middle of A8 segment), and S_2 in the middle of T2 segment. See the anatomy in Figure 1.
- For C-3PP, S_0 between 2 prolegs (in the middle of A8 segment), S_1 between A5-A6, and S_2 in the middle of T2 segment. Try to put them in the middle of the body height (between the surface - head/tail's top), also it is recommended that the Suction Cup's top must be inclined regarding the leg's/proleg's direction. See the anatomy in Figure 2.

STEP 2:

Define the length "B" between S_1 S_1 and S_2 (For C-PP and C-3PP), which is equal to "8 x L, where L is the measure of the link from S_0 to J_0 (for C-PP) and J_3 to S_2 (for both caterpillars).

STEP 3:

Lateral Joint (J_L) Location:

- For C-2PP, draw a circumference of diameter 2 x L at the Suction Cups' S_1 and S_2, then place J_1 at the right side of S_1 circumference, and J_2 at the left side of S_2 circumference. In addition, L has an angle of 90° formed with S_1 and S_2.
- For C-3PP, adding the procedure developed for C-2PP, then take the S_0-top and S_1-top as the center of a circumference (diameter 2 x L), where they are intersected, locate J_0.
- For both, at the center of J_1 and J_2, draw a circumference of diameter 6 x L Where both circumferences intersect, place the Joint J_2.

STEP 4:

Draw Links (L_i). Consider that links L form 90° with Suction Cups S_0, S_1 and S_2, which can be defined:

- For C-2PP, connect S_1 to J_1, J_1 to J_2, J_2 to J_3, J_3 to S_2.
- For C-3PP, connect S_0 to J_0, J_0 to S_1, S_1 to J_1, J_1 to J_2, J_2 to J_3, J_3 to S_2.

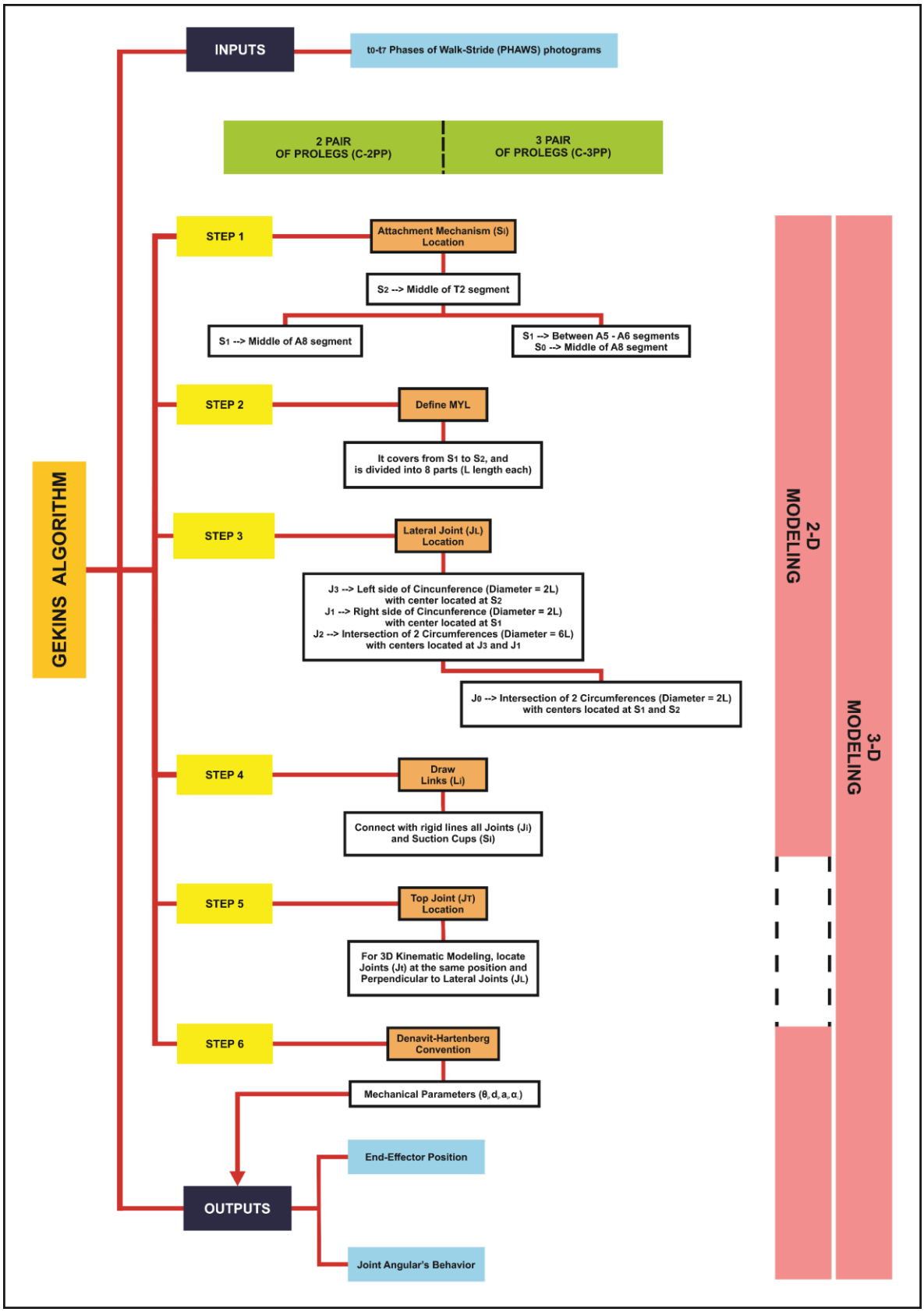

Figure 5. GEKINS algorithm, covering Input (PHAWS) / Output (end-effector position and joint angular's behavior) data, and the Steps (from the attachment mechanism location to the resulting parameters obtained by Denavit-Hartenberg convention) as well. Parameters in the diagram include: Suction Cups (S), MYL is the distance between Suction Cup *(S)* 1 to 2, Lateral Joint (J_L), Links (*Li*), Top Joint (J_T), and θ_i, d_i, a_i, α_i are the parameters for D-H convention. Parameters are summarized in Appendix 2, Table A.

STEP 5:

Top Joint (J_T) location:
- For both, place the DOF using a top view in the same location as J_L.

STEP 6:

The D-H convention is applied to obtain the table of parameters to define the geometry of the rigid body, which are for each joint [58]: θ, d, a, α. Regarding the angles θ, it is (+) positive when is formed rotating clockwise, but it is (-) negative when is formed rotating counterclockwise. The development of this convention, can be done according to the assigned values of θ_i and L_i shown in Figures 6 and 7, where 2 blocks of locomotion are defined during PHAWS: sequence H-T (the head is fixed and the tail location changes) and sequence T-H (the tail is fixed and the head location changes), so D-H parameters assigned in 2-D: "θ" are the values of θ_1, θ_2, θ_3 (for C-2PP), while θ_0, θ_1, θ_2, θ_3 (for C-3PP); "a" represents the values of L, L_1, L_2 (for C-2PP), while l, L_0, L_1, L_2 (for C-3PP); finally "d" and "α" are equal to 0. On the other hand, the D-H parameters assigned in 3-D: "θ" are the values of θ_1, θ_{T1}, θ_2, θ_{T2}, θ_3, θ_{T3} (for C-2PP), while θ_0, θ_{T0}, θ_1, θ_{T1}, θ_2, θ_{T2}, θ_3, θ_{T3} (for C-3PP); "d" values in H-T are L_{T1}, L_{T2}, but in T-H they are negative (for C-2PP), meanwhile in H-T are L_{T0}, L_{T1}, L_{T2}, but in T-H they are negative (for C-3PP); "a" represents the values of L, L_1, L_2 (for C-2PP), while L, L_0, L_1, L_2 (for C-3PP); and finally "α" represents in H-T the following sequence -π/2, π/2, -π/2, π/2, -π/2, 0, but in T-H they have the opposite signs (for C-2PP), meanwhile in H-T are -π/2, π/2, -π /2, π/2, -π/2, π/2, -π/2, 0, but in T-H they have the opposite signs (for C-3PP). Note that the current D-H convention uses the updated notations referred in the book titled Robotics, Vision and Control written by Peter Corke, et al [59, 60] which is based on the study performed by J. Denavit and R. S. Hartenberg in 1995 [61].

2.2.5. Biomechanical locomotion analysis in 2-D

To develop this analysis, the homogeneous transformation matrix was defined as "H" (equation 1):

$$\mathrm{H}_i = \begin{bmatrix} R_{3x3} & p_{3x1} \\ f_{1x3} & w_{1x1} \end{bmatrix} = \begin{bmatrix} Rotation & Traslation \\ Perspective & Scale \end{bmatrix}$$

$$\text{where } \boldsymbol{f}_{1x3} = [\mathbf{0}, \mathbf{0}, \mathbf{0}] \;\; ; \;\; \boldsymbol{w}_{1x1} = \mathbf{1}$$

$$\text{finally, } \mathbf{H_i} = \begin{bmatrix} \boldsymbol{R}_{3x3} & \boldsymbol{p}_{3x1} \\ \mathbf{0} & \mathbf{1} \end{bmatrix} \qquad (1)$$

Note that, the representation of these matrices is used to calculate the forward kinematics of the kinematic chains for both species of caterpillars [62].

2.2.5.1. End-Effector Position

The kinematic chain contains (depending on the specie): a) Suction Cups (S): S_0, S_1 S_2; b) joints: J_0, J_1, J_2 and J_3 (Revolute); c) links: L(2), L_0, L_1 and L_2. The motion process covers the formation of Angles: θ_0, θ_1, θ_2 and θ_3, which correspond to J_0, J_1, J_2 and J_3 respectively (Figures 6, 7, 11).

With the D-H parameters obtained in step 6 of GEKINS, now they can be applied for the end-effector position (X,Y,Z) of both caterpillars during locomotion analysis, which is proposed to be divided into 2 main blocks of walk-stride, were both sequences are defined using the H-M, to address the principles of forward kinematics, where the idea conception of a serial robotic manipulator (with base and EOAT) can be stated in comparison with caterpillars, as follows: a) sequence H-T, the EOAT is fixed and the base location changes, meanwhile b) sequence T-H, the base is fixed and the EOAT location changes. Therefore, for end-effector location purposes, it must be located at the part of the caterpillar/robot that is not fixed at sequence H-T/T-H.

a. Block 1: Sequence Head-Tail (H-T)

The caterpillar moves the prolegs while the legs are fixed (Block 1) – See Figures 1 and 2 to locate the caterpillar's anatomy. In addition, to understand the assigned values on the kinematic chain (θ_i and L_i) used on H-M, see Figures 6 and 7. This sequence covers the phases: t_0 - t_4 of walk-stride.

For C-2PP:
1. θ_3 is formed first.
2. Then, θ_2 is formed due to the prolegs (S_1) getting closer to the legs (S_2).
3. After that, θ1 is formed because of the prolegs' motion.

For C-3PP:
1. θ_3 is formed first.
2. Then, θ_1 and θ_2 are formed due to prolegs (S_0 and S_1) get closer to legs (S_2).
3. After that, θ_0 is formed because of the prolegs' motion.

In order to get the end-effector position (caterpillar's tail) that is located at S_1 (for C-2PP) and at S_0 (for C-2PP) during the walk-stride. The following computations (shown in equations 2 and 3) must be performed: a) Solution of the H-M which regards each joint-angle. b) Multiplication of H-M from H_3 to H_0 (depends on the insect's number of prolegs). c) Solution of End-Effector's position. Note that H-M are multiplied following the order: from H_3 to H_1 (for C-2PP), while from H_3 to H_0 (for C-3PP), then is added the L value in the X axis.

If $1 \leq i \leq 3$, use for both caterpillars. While if $i = 0$, then $L_{i-1}=L$ and use this only for C-3PP. So, the H matrix is represented by:

$$H_i = \begin{bmatrix} \cos\theta_i & -\sin\theta_i & 0 & L_{i-1}\cdot\cos\theta_i \\ \sin\theta_i & \cos\theta_i & 0 & L_{i-1}\cdot\sin\theta_i \\ 0 & 0 & 1 & 0 \\ 0 & 0 & 0 & 1 \end{bmatrix} \quad (2)$$

Therefore, the end-effector's position ("E") in 3-D cartesian coordinate system, is represented by:

$$E\begin{bmatrix} X \\ Y \\ Z \\ 1 \end{bmatrix} = H_3 \cdot H_2 \cdot H_1 \cdot H_0 \cdot \begin{bmatrix} 0 \\ 0 \\ 0 \\ 1 \end{bmatrix} + \begin{bmatrix} L \\ 0 \\ 0 \\ 1 \end{bmatrix} \quad (3)$$

b. Block 2: Sequence Tail-Head (T-H)

The caterpillar moves the legs while the prolegs are fixed (Block 2) – See Figures 1 and 2 to locate the caterpillar's anatomy. In addition, to understand the assigned values on the kinematic chain (θ_i and L_i) used on H-M, see Figures 6 and 7. This sequence covers the phases: t_5 - t_7 of walk-stride.

For C-2PP:

1. θ_1 is formed first.
2. Then, θ_2 is formed due to the legs (S_2) getting far from the prolegs (S_1).
3. After that, θ_3 is formed because of the legs' motion.

For C-3PP:

1. θ_0 is formed first.
2. Then, θ_1 and θ_2 are formed due to legs (S_2) get far from prolegs (S_0 and S_1).
3. After that, θ_3 is formed because of the legs' motion.

In order to get the end-effector position (caterpillar's head) that is located at S_2 (for both caterpillars) during walk-stride. The following computations (shown in equations 4 and 5) must be performed: a) Solution of the H-M which regards each joint-angle. b) Multiplication of H-M from H_0 to H_3 (depends on the insect's number of prolegs). c) Solution of End-Effector's position. Note that H-M are multiplied by the following order: from H_0 to H_2 (for C-2PP), while from H_0 to H3 (for C-3PP); then is added the L value in X axis.

If i = 0, use this only for C-3PP, or if $1 \leq i \leq 2$, use it for both caterpillars. While if i = 3, then Li=L and use for both caterpillars. So, the H matrix is represented by:

$$H_i = \begin{bmatrix} \cos\theta_i & -\sin\theta_i & 0 & L_i\cdot\cos\theta_i \\ \sin\theta_i & \cos\theta_i & 0 & L_i\cdot\sin\theta_i \\ 0 & 0 & 1 & 0 \\ 0 & 0 & 0 & 1 \end{bmatrix} \quad (4)$$

Therefore, the end-effector's position ("E") in 3-D cartesian coordinate system, is represented by:

$$E\begin{bmatrix} X \\ Y \\ Z \\ 1 \end{bmatrix} = H_0 \cdot H_1 \cdot H_2 \cdot H_3 \cdot \begin{bmatrix} 0 \\ 0 \\ 0 \\ 1 \end{bmatrix} + \begin{bmatrix} L \\ 0 \\ 0 \\ 1 \end{bmatrix} \quad (5)$$

2.2.5.2. Joint Angle's Behavior

This means the analysis of 2 parameters: angular - displacement (θ) and average velocity (ω). The values of θ present the motion process that covers the formation of 4 joint's angles: θ_0, θ_1, θ_2 and θ_3, which correspond to J_0, J_1, J_2 and J_3 respectively. Considering that each phase has 1 second, the angle displacement-equation can be obtained with the notation that angle data of PHAWS can be described as a straight line. Therefore, in order to get the average angular velocity, find the derivative of the angle displacement-equation.

2.2.6. Biomechanical locomotion analysis in 3-D

Then, following the last step of the GEKINS shown in Figure 5, now the D-H analysis is applied in 3-Dimensions. It consists of the joint location using a top view, so the final kinematic chain configuration contains dual rotational joints (DRJ), where in Figure 14: (a) means Block 1 (Sequence H-T) locomotion, and (b) means Block 2 (Sequence T-H) locomotion. Both blocks are represented by D-H parameters: "θ" are the values of θ_1, θ_{T1}, θ_2, θ_{T2}, θ_3, θ_{T3} (for C-2PP), while θ_0, θ_{T0}, θ_1, θ_{T1}, θ_2, θ_{T2}, θ_3, θ_{T3} (for C-3PP), we named as a TVA; "d" values in H-T are L_{T1}, L_{T2}, but in T-H they are negative (for C-2PP), meanwhile in H-T are L_{T0}, L_{T1}, L_{T2}, but in T-H they are negative (for C-3PP); "a" represents the values of L, L_1, L_2 (for C-2PP), while L, L_0, L_1, L_2 (for C-3PP); and "α" represents in H-T the following sequence $-\pi/2$, $\pi/2$, $-\pi/2$, $\pi/2$, $-\pi/2$, 0, but in T-H they have the opposite signs (for C-2PP), meanwhile in H-T are $-\pi/2$, $\pi/2$, $-\pi/2$, $\pi/2$, $-\pi/2$, $\pi/2$, $-\pi/2$, 0, but in T-H they have the opposite signs (for C-3PP).

Furthermore, these Joints are added: J_{T0} (for C-3PP), J_{T1}, J_{T2}, J_{T3} (for both species). Therefore, to obtain the digital kinematic chain representation, Matlab® with Robotics Toolbox developed by Peter Corke [48] was used (It is adapted to the variables used in GEKINS). Other simulation software can be used, such as: CoppeliaSim, ROS, GIM, ADAMS, etc.

Note that the analysis of joint's angular - displacement (θ) and average velocity (ω) was not developed in this section, because it is observed that the caterpillars have high flexibility on Top View Angles (TVA). Therefore, it is considered that there is no limited range for TVA, but with the purpose to reproduce on a robotic system, the limits can be added depending on each research.

3. Results

According to the data obtained using the GEKINS on the two caterpillar species (*Geometridae* and *Plusiinae*), in this section are described the most important comparisons between them based on 2-D and 3-D. It is important to define that each specie has the same kinematic chain from S_1 to S_2, which permits the comparison of J_1, J_2, J_3 and θ_1, θ_2, θ_3 of "*Geometridae* / *Plusiinae*". This means that *Plusiinae* has a back portion on its body that is different from *Geometridae*, and because of that reason, S_0 and J_0 belong to *Plusiinae*. Another feature regards that due to each specie has a different length, the re-scaling is proposed and applied to the analysis, getting the result that each insect has the same MYL dimension from S_1 to S_2, which is: 24 mm. In order to get better results that could be used as an input parameter for robot design and programming: each PHAWS (t_0-t_7) has 1 second of duration.

3.1. Biomechanical Locomotion Analysis in 2-D

3.1.1. Kinematic chain design

This process for both species is shown in Appendix 1 and Appendix 2 respectively, where the information is presented as follows: column "a"- the images of 8 locomotion (t_0-t_7) PHAWS, then column "b"- the location of the attachment mechanisms, joints and links, finally the column "c" – J_0, J_1, J_2, and J_3 location in 2-D (X,Y), where a coordinate grid composed of the X and Y axis is placed above from t_0 to t_7, where each square measures 100 mm x 100 mm, also the scale is 1:100.

As it is shown in Appendix 1, for *Geometridae*, the WSL measures 14,43 mm (From t_0 Phase – S_2 Suction Cup location to t_7 Phase – S_2 Suction Cup location) and MYL in real life is 22 mm, while in adjusted scale is 24 mm. Also, in Appendix 2, for *Plusiinae*, the WSL measures 13,82 mm (From t_0 Phase – S_2 Suction Cup location to t_7 Phase – S_2 Suction Cup location) and MYL in real life is 20 mm, while in adjusted scale is 24 mm. Note that in t_0 Phase, S_0 starts in (0,0).

3.1.2. Joint (J_L) location

The data shown in Appendix 3 – Table B is about the specific locations of each insect during locomotion (based on Figures 6c and 7c), which is used to present 3 graphics about joint location, considering that the kinematic chain of "*Geometridae* – from Joint 1 to Joint 3" is the similar to "*Plusiinae* – from Joint 1 to Joint 3": Figure 6a) J_1 (*Geometridae*) vs J_1 (*Plusiinae*), getting the result of *Geometridae*'s joint is located ahead of *Plusiinae*'s joint in each phase, and equals in t_0. Figure 6b) J_2 (*Geometridae*) vs J_2 (*Plusiinae*), getting the result of *Geometridae*'s joint is located ahead of *Plusiinae*'s joint in each phase, except in t_5 and t_6, and equals in t_0. Figure 6c) J_3 (*Geometridae*) vs J_3 (*Plusiinae*), getting the result of *Geometridae*'s joint is located behind *Plusiinae*'s joint in t_5 and t_6, ahead of *Plusiinae*'s joint in t_7, and equals from t_0 to t_5. Therefore, regarding the stride length of each insect: the *Geometridae* got 14.43 mm, and *Plusiinae* got 13.82 mm, which shows that the stride path of *Geometridae* is greater.

Additionally, in Appendix 3 – Table B is presented the joint values of t_0 = (0,0) – (X, Y), due to the values of each phase are subtracted by the value of t_0 shown in Appendix 1 and Appendix 2.

Regarding the information presented in Figure 6, the joint location during a walk-stride is shown, the axis are X-Y and the measurements are in millimeters. As it is shown in Appendix 3 – Table B, and in Figure 6, J_1 for *Geometridae* finishes at 14.86 mm-X and 0.00 mm-Y, and achieves the maximum peak at (t_4) 14.86 mm-X and 1.68 mm-Y, whereas for *Plusiinae* finishes at (t_4) 13.76 mm, and achieves the maximum peak at 13.45 mm-X and 1.91 mm-Y. Also, J_2 for *Geometridae* finishes at 14.65 mm-X and 1.31 mm-Y, and achieves the maximum peak at (t_5) 7.84 mm-X and 7.99 mm-Y, whereas for *Plusiinae* finishes at 13.79 mm-X and -0.13 mm-Y, and achieves the maximum peak at (t_4) 10.32 mm-X and 7.17 mm-Y. Finally, J_3 for *Geometridae* finishes at 14.43 mm-X and 0.00 mm-Y, and achieves the maximum peak at (t_5) 7.05 mm-X and 5.03 mm-Y, whereas for *Plusiinae* finishes at 13.82 mm, and achieves the maximum peak at (t_5) 10.05 mm-X and 6.40 mm-Y.

In summary, when comparing kinematic chains for *Geometridae* and *Plusiinae*, it is observed that:

- Both species have the same kinematic chain from S_1 to S_2, which permits the comparison of J_1, J_2, J_3 and θ_1, θ_2, θ_3 of both insects.
- The back portion of the body and the length is higher for *Geometridae* (22 mm) than for *Plusiinae* (20 mm).
- The WSL is greater for *Geometridae* (14.43 mm) than for *Plusiinae* (13.82 mm)
- *Geometridae*'s joint is located behind *Plusiinae*'s joint in T_5 and T_6, equal in T_0 to T_5, but in T_7 the *Geometridae* is ahead.

3.1.3. D-H convention

a. Kinematic modeling for sequence H-T

According to the data of t_0-t_4 in Figures 6 and 7, the D–H convention was applied, where frames and parameters can be shown in Appendix 4 – Table C and Figure 7 respectively. The base of the robot is placed at the right side (end of L next to J_3), meanwhile, the end-effector is located at the left side "X_3-Y_3" frame for *Geometridae* and "X_4-Y_4" frame for *Plusiinae.* Note that D-H parameters θ_i, d_i, a_i, α_i are described in section 2.2.4.

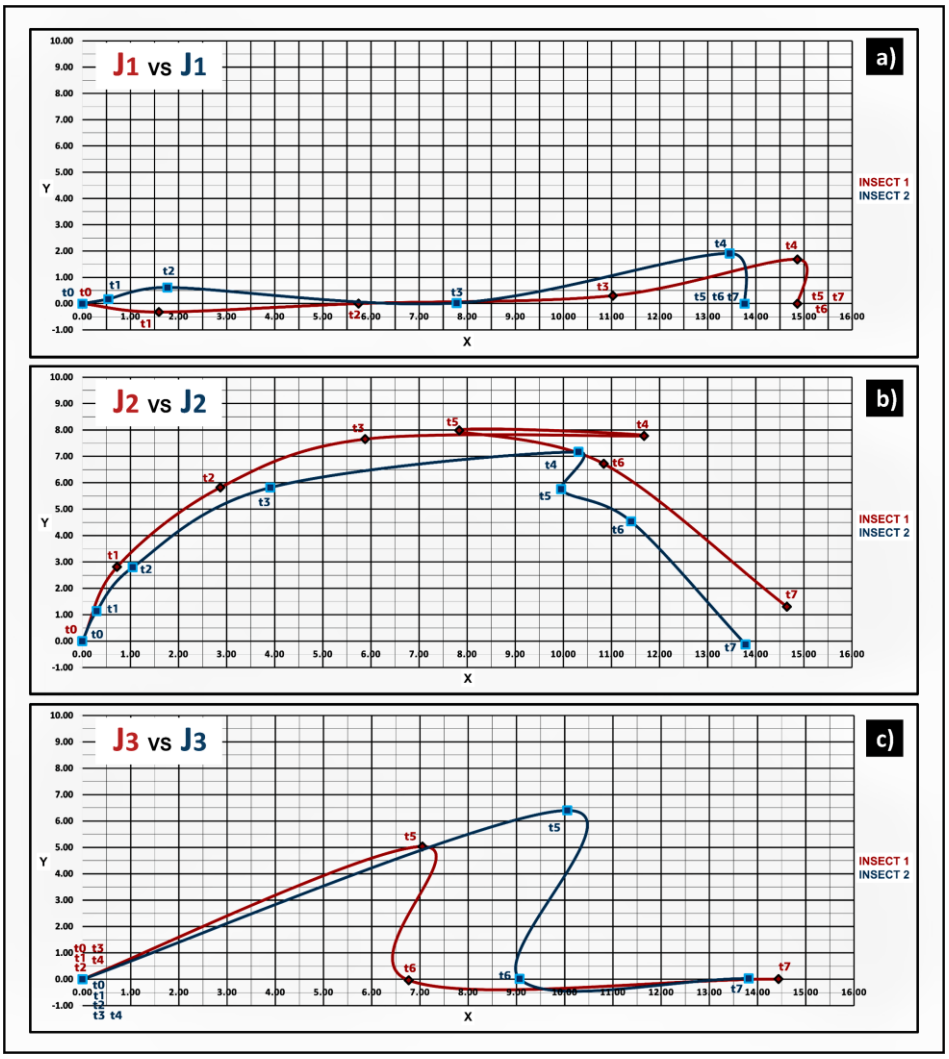

Figure 6. Comparative joint location. a) J_1, b) J_2, c) J_3. Note that Insect 1 is *Geometridae* and Insect 2 is *Plusiinae*. Note that axes units are measured in mm.

b. Kinematic modeling for sequence T-H

According to the data of t_5-t_7 in Figures 6 and 7, the D–H convention was applied, where frames and parameters can be shown in Appendix 5 – Table D and Figure 8 respectively. The base of the robot is placed at the left side (end of *L* next to J_1 for *Geometridae*, and J_0 for *Plusiinae*), meanwhile, the end-effector is located at the right side "X_3-Y_3" frame for *Geometridae*, and "X_4-Y_4" frame for *Plusiinae*). Note that D-H parameters θ_i, d_i, a_i, α_i are described in section 2.2.4.

3.1.4. Joint Angle's Behavior

a. Joint angle displacement (θ)

It is shown in Appendix 6 – Figure B for (i) *Geometridae* and (ii) *Plusiinae*, where the information is presented as follows: column "a"- the images of 8 locomotion (t_0-t_7) PHAWS, then column "b"- kinematic chain locomotion, and finally column "c" – angular displacement in degrees of each Joint. Note that the Joint angle's behavior covers the angular displacement (θ_i) and average angular velocity (ω_i).

According, Figure 9: For (i) *Geometridae*, the motion process covers the formation of 3 Angles: θ_1, θ_2 and θ_3, which correspond to J_1, J_2 and J_3 respectively. In addition, it is shown that θ_1 range is from 5.10° to 77.56°; θ_2 range is from -10,22° to -157.38°; and θ_3 is from 5.11° to 107.55° (Appendix 6 – Figure B). For (ii) *Plusiinae*, the motion process covers the formation of 4 Angles: θ_0, θ_1, θ_2 and θ_3, which correspond to J_0, J_1, J_2 and J_3. In addition, it is shown that θ_0 range is from -21.95° to 18.40°; θ_1 range is from 10.15° to 65.02°; θ_2 range is from -150.19° to -20.10°; and θ_3 range is from 9.37° to 99.47° (Appendix 6 – Figure B).

The comparison about angular displacement (θ_i) of *Geometridae*, and *Plusiinae* is shown in Appendix 7 – Table E. Additionally, in Figure 9a) θ_1, *Geometridae* has a minimum value of 5.10° in t_0 and a maximum value of 77.56° in t_5, whereas *Plusiinae* has 10.15° in t_7 and a maximum value of

65.02° in t_3. In Figure 9b) θ_2, *Geometridae* has a minimum value of -10.22° in t_0 and a maximum value of -157.58° in t_4, whereas *Plusiinae* has -20.10° in t_7 and a maximum value of -150.19° in t_4. In Figure 9c) θ_3, *Geometridae* has a minimum value of 5.11° in t_0 and a maximum value of 107.55° in t_4, whereas *Plusiinae* has 9.37° in t_7 and a maximum value of 99.47° in t_4. So, regarding this information, *Geometridae*, shows minimum values in t_0 and maximum values in t_5 (θ_1) and t_4 (θ_2, θ_3), and *Plusiinae* shows minimum values in T_7 and maximum values in t_3 (θ_1) and t_4 (θ_2, θ_3). Therefore, the observable main result is that *Geometridae* and *Plusiinae* have maximum angle values of θ_2 and θ_3 in t_4.

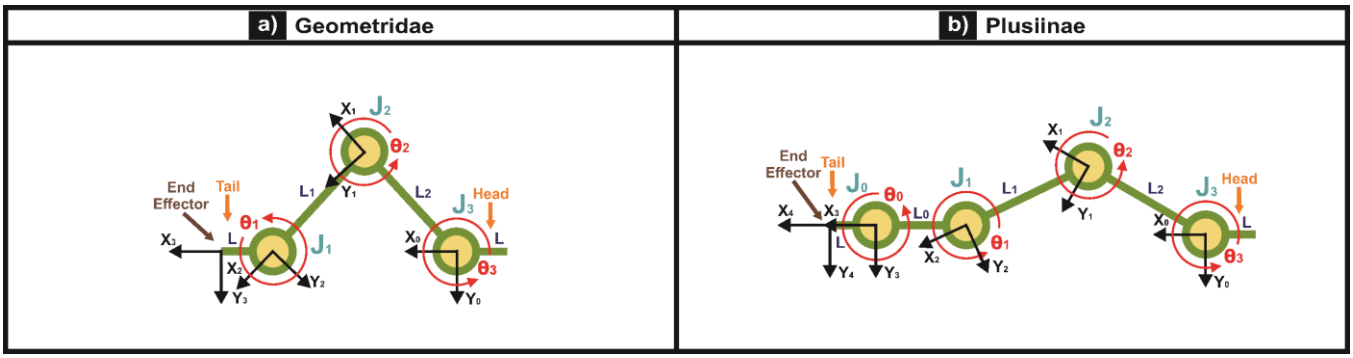

Figure 7. D-H frames of Kinematic Chain (2-D) for the locomotion: Sequence H-T: a) *Geometridae* and b) *Plusiinae*.

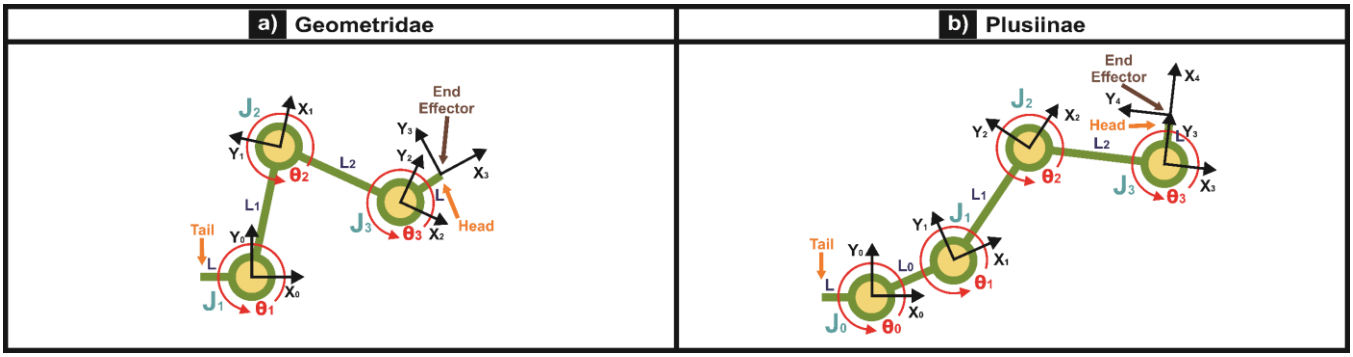

Figure 8. D-H frames of Kinematic Chain (2-D) for the locomotion: Sequence T-H: a) *Geometridae* and b) *Plusiinae*.

b. Joint angular average velocity (ω)

Taking into account that each phase has 1 second, and after the analysis of the graphics presented in Figure 9, the angle displacement-equation can be obtained with the notation that angle values in each phase (From t_0 to t_7) can be described as a straight line. Therefore, in order to get the equations, the slope and x/y axes intercept of each phase had to be resolved (Linear Interpolation), the results are shown in Appendix 8 – Table F. That information is useful to know that the angular displacement (θ_0) described in each joint is proportional to the time increment/decrement. In addition, to obtain ω_i, find the derivative of the angular displacement-equations before mentioned.

As it is shown in Appendix 8 – Table F, regarding the angular average velocity (ω_i) of:

1. *Geometridae*: J_1 shows a range from -43.14 to 45.81 °/s, J_2 shows a range from -45.18 to 86.76 °/s, J_3 shows a range from -51.06 to 37.60 °/s.
2. *Plusiinae*: J_0 shows a range from -20.88 to 40.35 °/s, J_1 shows a range from -33.80 to 39.39 °/s, J_2 shows a range from -57.63 to 87.31 °/s, J_3 shows a range from -34.20 to 42.67 °/s.

As shown in Appendix 8 – Table F, regarding the angular average velocity (ω_i), *Geometridae* joint J_1 shows a range from -43.14 to 45.81 °/s, J_2 shows a range from -45.18 to 86.76 °/s, and J_3 shows a range from -51.06 to 37.60 °/s. For *Plusiinae*, joint J_0 shows a range from -20.88 to 40.35 °/s, J_1 shows a range from -33.80 to 39.39 °/s, J_2 ranges from -57.63 to 87.31 °/s, and J_3 ranges from -34.20 to 42.67 °/s.

3.2. Biomechanical Locomotion Analysis in 3-D

3.2.1. D-H convention

In order to perform a 3-D analysis, the top views are shown in Figure 10, where the images are selected because they show anatomical high flexibility of both species. Then, keeping the same variables used until step 4 of GEKINS, now the Top View Angles (TVA) are added: θ_{T0}, θ_{T1}, θ_{T2} and θ_{T3}; Joints: J_{T0}, J_{T1}, J_{T2}, J_{T3}; and Links: L_{T0}, L_{T1}, L_{T2} (θ_{T0}, J_{T0}, and L_{T0} only for *Plusiinae*). Both blocks of walk-stride are represented by D-H parameters in Figure 11 and Appendix 9 – Table G, where is

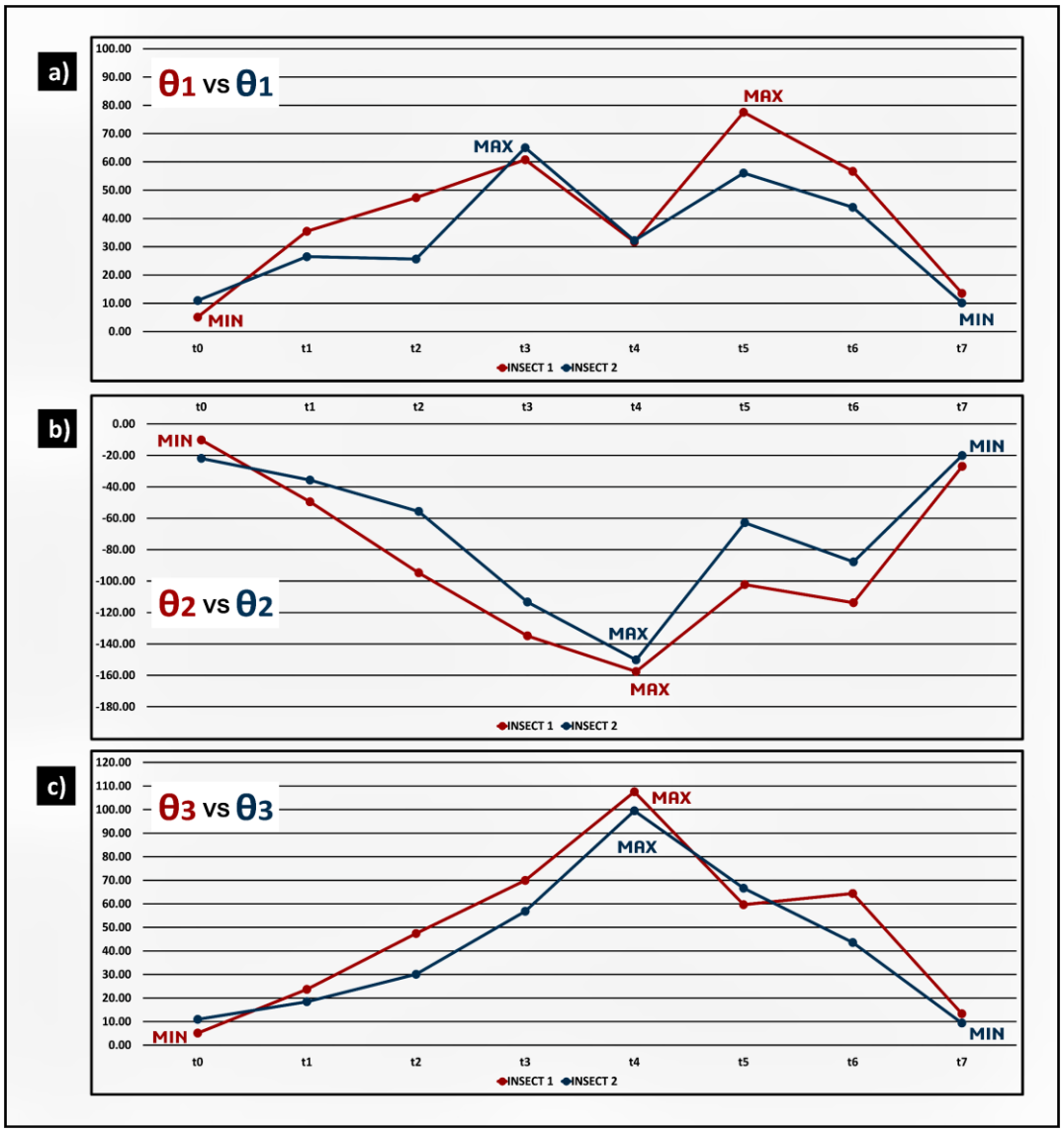

Figure 9. Comparative Angle Displacement. a) $\theta 1$, b) $\theta 2$, c) $\theta 3$. Note that Insect 1 is *Geometridae* and Insect 2 is *Plusiinae*. Note that Y axis unit is (°).

shown that the kinematic chain has 6 DOF (3 DOF – Dual Rotational Joints) for *Geometridae*, and 8 DOF (4 DOF – Dual Rotational Joints) for *Plusiinae* (Figure 10).

The angle between the two shafts of dual rotational joints (DRJ) was determined by experimental observation. Due to the flexible nature of the inching-locomotion caterpillar (ILAR), performing an accurate measurement of this angle using video processing would have been very complex. However, using top view images of specimens was checked that this angle can be approximated to 90° degrees. Besides these 90° degrees angle facilitate the future construction of the robot and the implementation of industrial applications. DRJ were located following locomotion photograms per each specie (Appendix 1 – Figure A.1 and Figure A.2)

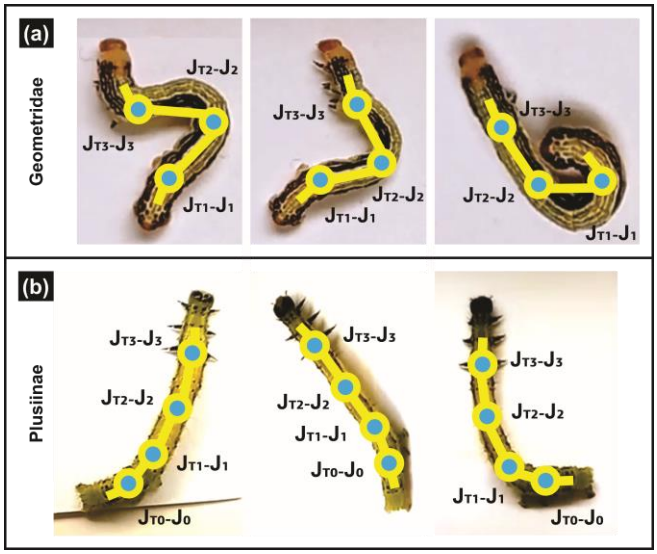

Figure 10. Top views of a) *Geometridae* and b) *Plusiinae* Kinematic Chains.

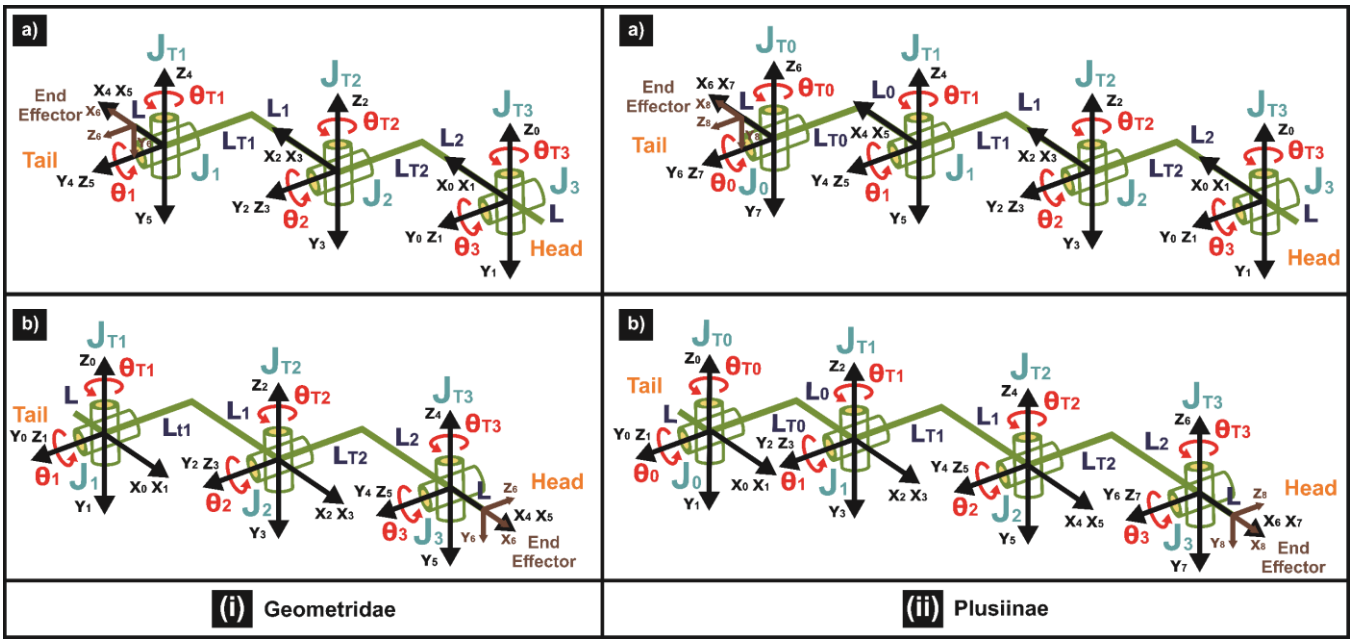

Figure 11. *Geometridae* (i) and *Plusiinae* (ii) Kinematic Chains (3-D). D-H convention applied on Locomotion: a) Sequence H-T, b) Sequence T-H.

3.2.2. Graphical simulation

According to step 6 of GEKINS – Figure 5, the proportional dimensions of the links are: L_0=2*L* (Only for *Plusiinae*), L_1=3*L* and L_2= 3*L* (For both caterpillars). So, in order to obtain the digital kinematic chain 3-D representation, Matlab® with Robotics Toolbox was used, where SerialLink code was applied to implement the steps shown in Appendix 10 – Table H, where the data is adapted to the variables used in Appendix 9 – Table G. Therefore, the 3-D Kinematic Model is presented in Figure 13 showing the PHAWS of each caterpillar-robot.

3.3. Degrees of Freedom (DOF) in 2-D and 3-D

Using the D-H convention, kinematic modeling in 2-D and 3-D was possible. In addition, the simulation algorithms based on SerialLink() were coded in Matlab®. Regarding *Geometridae*, in 2-Dimensions, it has 3 DOF, and in 3-Dimensions, it has 6 DOF (3 DOF – Dual Joints). On the other hand, *Plusiinae*, in 2-Dimensions, it has 4 DOF, and in 3-Dimensions, it has 8 DOF (4 DOF – Dual Joints). The joints are rotational type, note that for 3-D development they can be implemented by universal joints. The kinematic chains have been figured out with outstanding precision for rigid links for inching-locomotion caterpillars.

3.4. Quantitative Comparison of Kinematic Chains

The Key Performance Indicators (KPIs) of this study lie in developing 6 main characteristics (shown in Table 1) for comparing locomotion between ILAR.

Fastest Angular Velocity (FAV): a fast angular velocity means the need of an actuator with high performance; thus, it is preferable low values in this indicator to reduce the design requirements. This metric is measured in deg/s.

Gait Velocity (GV): a walking ability that measures distance traveled divided by the time taken. In principle, robots with larger kinematic chains will move faster, thus the velocity will depend on the scale of the robot. To perform a comparison unaffected by the scale, this velocity is divided by the length of the kinematic chain. It is desirable to have a large value in this metric. This metric is measured in s^{-1}.

Workspace (WSP): a characterization of the reachable configuration's locations of the end-effector. This is used to compute the Area of Workspace (AWSP).

Area of the WorkSpace (AWSP): In order to obtain a numeric value, the total area of the WSP is computed. Again, in order to perform a comparison unaffected by the scale, this area is divided by $\pi(KCL)^2$, where KCL is the length of the kinematic chain. Robots with larger WSPs are preferred. This metric is dimensionless.

Maximum Working Range (MWR): is the distance to the point most separated in the space in which the robot's task can most naturally be expressed WSP. In order to perform a comparison unaffected by the scale, this metric is divided by the length of the kinematic chain. Robots with larger MWRs are preferred. This metric is dimensionless.

Maximum Obstacle's Height (MOH): denotes the ability of the robot to move around obstacles and it measures how the maximum obstacle's height that can be overpassed.

Table 1. KPIs of Kinematic Chains

FAV	$\boldsymbol{FAV = MAX\left(w_j(t_i)\right)\ \ t_i \in \{t_0,..,t_7\}, j \in \{0,..,3\}}$ *Appendix 8 – Table F.
GV [s^{-1}]	$GV = \frac{WSL}{\Delta t \cdot KCL}$ Δt means total time of walk stride from t_0 to t_7
WSP	$\boldsymbol{WSP} = (x,y) \in \mathbb{R}^2 \mid \boldsymbol{E(\theta_0,..,\theta_3).xy}$, $\boldsymbol{\theta_0} \in \{\boldsymbol{k} \in \mathbb{R} \mid \lvert\boldsymbol{k}\rvert \leq \boldsymbol{2\pi}\}, \ldots, \boldsymbol{\theta_3} \in \{\boldsymbol{k} \in \mathbb{R} \mid \lvert\boldsymbol{k}\rvert \leq \boldsymbol{2\pi}\}$,
AWSP	$\boldsymbol{f_{WSP}(x,y)} = \begin{cases} \boldsymbol{1}, & \boldsymbol{(x,y) \in WSP} \\ \boldsymbol{0}, & \boldsymbol{(x,y) \notin WSP} \end{cases}$ $\boldsymbol{AWSP = \frac{1}{\pi KCL^2} \int\int f_{WSP}(x,y) dxdy}$ *Appendix 1 – Figure A.1 and Figure A.2
MWR	$\boldsymbol{MWR = \frac{1}{KCL} MAX\left(\sqrt{x^2+y^2}\right)}$, $\boldsymbol{(x,y) \in WSP}$
MOH	$\boldsymbol{MOH = \frac{1}{KCL} MAX(y)}, \quad \boldsymbol{(x,y) \in WSP}$ *Appendix 1 – Figure A.1 and Figure A.2.

Following the analysis performed in Table 1, quantitative data has been obtained, which means that KPIs were correctly validated (shown in Table 2). In this particular case, we used those metrics, but it depends on the researcher's interests. Note that Kinematic Chain Length (KCL) is defined as MYL for *Geometridae*, and as MYL + 2**L₀* for *Plusiinae* – shown in Appendix 1.

Table 2. KPIs Comparison for ILAR

	Geometridae (C-2PP) (KCL = 24 mm)	*Plusiinae* (C-3PP) (KLC = 30 mm)
FAV	J_2 (86.7 °/s)	J_2 (87.31 °/s)
GV	0.086 s^{-1}	0.066 s^{-1}
AWSP	7.96×10^{-5}	5.31×10^{-5}
MWR	0.619	0.459
MOH	0.478	0.338

Besides, the workspace (WSP) analysis has been performed following the walk-stride locomotion using Matlab® [63], to get an understanding of the end-effector's reachability location that is on the head of caterpillars (Appendix 11 - Figure C.1. and Figure C.2.). Taking into account the proportional length of links (Appendix 12 – Table I): A). For *Geometridae* it is observed that the end-effector could reach the highest point (x=0.096m, y= 0.684m), B) For Plusiinae it is observed that the end-effector could reach the highest point (x= 0.179m, y=0.769m). Also, this caterpillar covers a major surface of WSP-reachability than the *Geometridae*.

In order to evaluate the feasibility of the construction of future robots which follow the proposed kinematic chains, parameters for the masses and the inertias have been designed, then the maximum angular speed and maximum torque have been computed. From these values it has been checked that in the market there are actuators which fit these requirements.

For instance, for the *Geometridae* the following realistic assumptions can be done for joints 1 and 2: the length is 0.9 m, the center of mass is 0.45 m, the mass is 0.3 Kg, the inertia is 0.02 $kg.m^2$, and for the joint 3: the length is 0.3 m, the center of mass is 0.15 m, the mass is 0.1 Kg, and the inertia is 0.0008 $kg.m^2$, so under these assumptions the maximum torque and angular speed are 27.24 Nm and 1.3 rad/s.

Following similar assumptions for the *Plusiinae* the maximum angular speed ant torque are 22.59 Nm and 1.80 rad/s. All these values are not too high; thus, it is realistic to find actuators in the market that fit these requirements. Therefore, the construction of robots which match these kinematic chains is feasible.

4. Discussion

The main objective of the GEKINS algorithm is to identify experimentally bio-inspired kinematic models from videos of moving caterpillar specimens. To achieve this aim, this work standardizes the proportional dimensions of kinematic chains for inching-locomotion caterpillars (ILAR). This manuscript aims to show how to standardize the kinematic chain definition with the use of a geometrical method (BIROD and GEKINS) for arthropod animals in order to build a robot in the future. In this context, we proposed the study of ILAR, so, we selected the 2 only family-groups that perform this type of gait: *Geometridae* (it represents 35,000 species) [64] and *Plusiinae* (it represents 400 species) [65].

Besides, a comparative analysis between the kinematic chains obtained from two different species (*Geometridae* and *Plusiinae*) has been carried out, taking into account: kinematic models and the stride length, D-H parameters, angles of rotation–angular displacement, and finally the average velocity by each joint. To compare these kinematic models a comprehensive set of metrics have been proposed that considers, among other things, the reachability and the obstacle avoidance ability. This analysis is done in order to

use these kinematic chains for future works applying to symbiotic design on mechatronic machines, and taking into consideration the features of reconfigurability and modularity. Furthermore, a locomotion study of *Plusiinae* was presented; to the best of our knowledge, the motion of this species had not been previously studied for bio-inspired robot design. It has some morphological-technical characteristics that mark a great potential to be used in robotics.

Therefore, results from this study indicate that the application of the proposed GEKINS algorithm permits to locate in both caterpillars two to three Suction Cups (S_0 and S_2 for *Geometridae*, and S_1 and S_2 for *Plusiinae*), three to four Joints (J_0, J_1, J_2 and J_3), and three to four Links (L, L_0, L_1 and L_2) and eight (t_0 to t_7) PHAWS that have 1 second of duration each. Moreover, permits to calculate the WSL, the angular displacement (θ), the angular average velocity (ω) by each joint, and the number of Dual Rotational Joints (DRJ) by each DOF in 2-D and 3-D. In addition, when comparing both species with this method some differences were found: Each species has the same kinematic chain from S_1 to S_2, which permits the comparison of J_1, J_2, J_3 and θ_1, θ_2, θ_3 of both insects. Also, the WSL is greater for *Geometridae* (14.43 mm) than for *Plusiinae* (13.82 mm), however, *Geometridae*'s joint is located behind *Plusiinae*'s joint in T_5 and T_6 and equals in T_0 to T_5, but in T_7 the *Geometridae* is ahead. Moreover, both insects have maximum angular displacement/angle velocity values of θ_2 and θ_3 in t_4. Hence, the angular average velocity (ω_i) is higher for *Geometridae* in J_1, lower for J_2, and higher for J_3. Additionally, the number of links is lower for *Geometridae* (4) than for *Plusiinae* (5). Furthermore, the number of DOF is lower for *Geometridae* than for *Plusiinae* in two (3 DOF versus 4 DOF) and three dimensions (6 DOF versus 8 DOF) respectively. All these joints can be implemented as a universal joint, which can be useful for the design of reconfigurable and modular robots [60, 66].

Thus, related to the geometric features of kinematic chains, *Geometridae*'s (C-2PP) shape can be suited for assembly tasks of blocks, having a locomotion walk-stride comparable to the Bill-e robot developed by MIT and NASA [67], however, the *Plusiinae*'s (C-3PP) shape can be adapted for in-pipe exploration, comparable to the system developed in the PIRATE project at IMPACT Institute, University of Twente [68]. Moreover, regarding KPIs metrics, it can be observed that: i) FAV: J_2 is the fastest joint for both species, but C-3PP achieves a greater value. ii) GV: C-2PP performs a fastest gait than C-3PP. iii) AWSP C-2PP has a greater WSP than C-3PP. iv) MWR: C-2PP shows a greater reachability than C-3PP. v) MOH: C-2PP has the ability to avoid a larger obstacle than C-3PP. To sum up, we can conclude that C-2PP covers better functionalities for locomotion and even manipulation tasks. The next step of this project includes developing a reconfigurable system that integrates both, C-2PP and C-3PP kinematic chains, useful for industrial applications, that covers assembly and manipulation tasks, and controlled locomotion for exploration at tight and limited access environments [69].

ILAR do not utilize their legs and prolegs to drive themselves forward. In contrast, they serve as anchors, keeping them firmly in place when body segments move, for example, when they attach to a stiff substrate, such as a twig. That twig functions as an exterior skeleton, providing the stability caterpillars require to tense their muscles [70]. So, following the aforementioned statement, GEKINS algorithm finds the locations of the legs and prolegs in order to be replaced by Suction Cups (S), for this reason, C-2PP has 2 Suction Cups, while C-3PP has 3. There is a general tradeoff between the flexibility offered by more pairs of legs versus the complexity of controlling more of them. It would be interesting to further understand how these animals evolved in relation to their locomotion.

There are 2 biological studies about caterpillar locomotion published in 1997 and 1999 [71-73], but only 2 projects related to an engineering kinematic analysis: a) 1 published in 2008 by the University of Tabriz [33], which stated that the body of the caterpillar can be represented by 5 links, and b) 1 developed by the Robotics Institute at Beihang University with the Department of Computer Science at the University of Hamburg, which started with 2 publications in 2008 and 2009 and established a basic kinematic chain of an Inch-Worm, composed by 4 links [34, 35]. Both projects previously mentioned are only applied for *Geometridae* (which represents a caterpillar with 2 pairs of prolegs). Now, our current study lies on the experimental study based on a new methodology proposed for standardizing the proportional dimensions related to inching-locomotion caterpillar's (*Geometridae* and *Plusiinae*) morphology, to get the features to perform that motion when it will be integrated into a robot design. Therefore, following the former kinematic analysis [34, 35], it shows a locomotion of 1 walk-stride divided into 5 phases (T_0-T_5): T_0, T_1, T_2, T_3, T_4 (Figure 12) [34, 35], on the other hand, our research shows 8 phases (t_0-t_7), where the phases T_0, T_1, T_2, T_3, T_4 [34, 35] are equivalent to t_0, t_1, t_3, t_5, t_7 respectively (Appendix 1, 2, and 6).

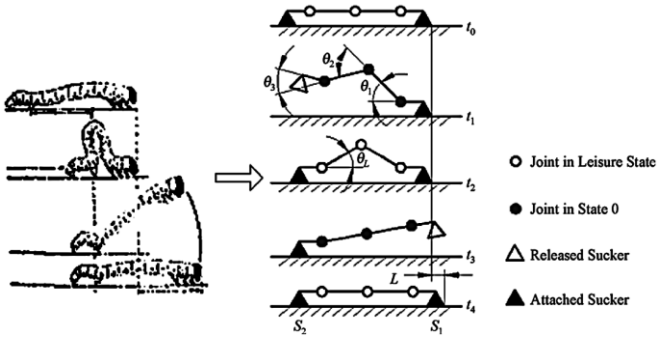

Figure 12. Gait and Kinematic Model of Inch-Worm (*Geometridae*).

Finally, there are several strengths of this study. 1) To our knowledge, it is the first and unique academic original article, where BIROD method is presented to design kinematic chains based on observational analysis of ILAR, taking videos and photos to understand their biomechanics. 2) The proposed GEKINS algorithm is the only one applied for kinematic modeling of ILAR species, having 2 options (Figure 5): "2-CPP" for those which have 2 pair of prolegs (*Geometridae* – Figure 1) and "3-CPP" for those which have 3 pair of prolegs (*Plusiinae* – Figure 2). 3) The method is focused on the creation of a system to be able to reproduce a similar gait (PHAWS) to the real animal, so in order to check the accuracy of the model, we state that the joint 2 (J_2) indicates the flexibility of the kinematic chain due to its greater range of motion, which should be located in the middle of A3 anatomical segment (Figure 2). 4) A comparative test was performed to validate the GEKINS algorithm on *Plusiinae* (Appendix 13 – Figure D), which consisted of using the 2 options (Figure 5): 2-CPP (which is used for *Geometridae*) and 3-CPP, concluding that the use of 3-CPP is the best option to develop an accurate kinematic chain model of species with 3 pair of prolegs, because J_2 is located closer to the A3 segment (Appendix 13 – Table J).

5. Conclusion and future works

In this paper, the objective is to analyze the locomotion and kinematic chain of two main groups of ILAR species. The GEKINS algorithm was developed to standardize the proportional dimensions according to the insect's anatomy for the experimental study of kinematic chain modeling, which is part of a novel Bioinspired Robotic Design (BIROD) method. The obtained data indicate that the application of the proposed method permits to locate the attachment mechanisms (S), joints (Ji), links (Li), and to calculate angular displacement (θ), angular average velocity (ω), and number of DOF.

When comparing the two species, both insects have similar anatomy characteristics, however, some features make them different, thus, key performance indicators (KPIs) were used to define 6 metrics: FAV, GV, MWR, WSP, AWSP, MOH, resulting on quantitative data that can be used to select the best robotic application. Furthermore, *Geometridae* in contrast of *Plusiinae*, it has a lower number of single-rotational joints in 2-D (3 DOF versus 4 DOF), and a lower number of dual-rotational joints in 3-D (6 DOF versus 8 DOF). The rotational joints can drive the motion of the robot based on rotary electro-mechanical motors. Motor sizing will be considered in future works.

In the case of someone who would like to create a robot inspired by ILAR, our research had already covered the kinematic chain modeling, it is expected to be useful as a preliminary phase for the design of bio-inspired robots. Additionally, this academic paper covers until forward kinematics and workspace development. The results are expected to be valid for all species of ILAR, and must be adapted according to the length of the species, because they perform similar walk-stride motion: shrink the abdominal segments, almost reaching the prolegs with legs, during crawling.

In future work, the performance of the kinematic chains will be evaluated with real robots, moreover, the incorporation of parameters related to multi-body dynamics such as inertia and mass will be considered for a more detailed ILAR species comparison. We plan as future work also to consider the applications regarding autonomous multi-robot systems - AMRS / collective robotic construction - CRC, including the classification of objects and placement at optimal locations using modularity and swarm foundations, as these robots may be useful for industrial assembly, limited access inspection and space construction (Moon and Mars). Finally, the proposed methodology could be adapted to the design of kinematic chains for other arthropods animals, which can also be useful in the design of reconfigurable and modular robots.

Highlights

- BIROD method and GEKINS algorithm are implemented to introduce a novel gait analysis in 2-D and 3-D of inching-locomotion caterpillars to develop bio-inspired robots.
- Key performance indicators are defined to compare the kinematic chains of inching-locomotion caterpillars, which could be adapted to design other arthropod robots.
- The results generalize to 35,400 species of inching-locomotion caterpillars from *Lepidoptera* family, where *Geometridae* represents 35,000 (2 pair of prolegs), and for *Plusiinae* represents 400 (3 pair of prolegs).

Declaration of Competing Interest

The authors declare that they have no known competing financial interests or personal relationships that could have appeared to influence the work reported in this paper.

Data availability statement

The data that support the findings of this study are available upon request from the authors.

Acknowledgment

The authors are deeply grateful to the staff of Universidad Nacional Agraria La Molina for supporting the collection of caterpillar specimens. A great thanks to Tamara Cole for designing Figures 1 and 2. Also, thank the anonymous reviewers for all the useful and helpful comments on our manuscript.

Abbreviations

AWSP: **A**rea of the **W**ork**SP**ace
BIROD: **Bi**oinspired **Ro**botic **D**esign
C-2PP: **C**aterpillars with **2** **P**airs of **P**rolegs
C-3PP: **C**aterpillars with **3** **P**airs **of** **P**rolegs
D-H: **D**enavit-**H**artenberg
DOF: **D**egrees **o**f **F**reedom
DRJ: **D**ual **R**otational **J**oints
EOAT: **E**nd **o**f **A**rm **T**ooling
FAV: **F**astest **A**ngular **V**elocity
GV: **G**ait **V**elocity
GEKINS: **Ge**ometrical **Kin**ematic **A**nalysi**s**
H-T: **H**ead-**T**ail
H-M: **H**omogeneous **M**atrix
ILAR: **I**nching-**L**ocomotion **C**aterpill**ar**
KCL: **K**inematic **C**hain **L**ength
KPIs: **K**ey **P**erformance **I**ndicators
MWR: **M**aximum **W**orking **R**ange
MYL: **M**ain Bod**y** **L**ength
MOH: **M**aximum **O**bstacle's **H**ight
PHAWS: **P**hases of **W**alk-**S**tride
T-H: **T**ail-**H**ead
TVA: **T**op-**V**iew **A**ngles
WSL: **W**alk-**S**tride **L**ength
WSP: **W**ork**sp**ace

ORCID iDs

José Cornejo
https://orcid.org/0000-0003-4096-9337

J. Enrique Sierra-Garcia
https://orcid.org/0000-0001-6088-9954

Francisco Javier Gomez-Gil
https://orcid.org/0000-0003-0586-7271

Juan Grados
https://orcid.org/0000-0002-2277-3616

Ricardo Palomares
https://orcid.org/0000-0001-9076-3674

Alfredo Weitzenfeld
https://orcid.org/0000-0001-7016-3751

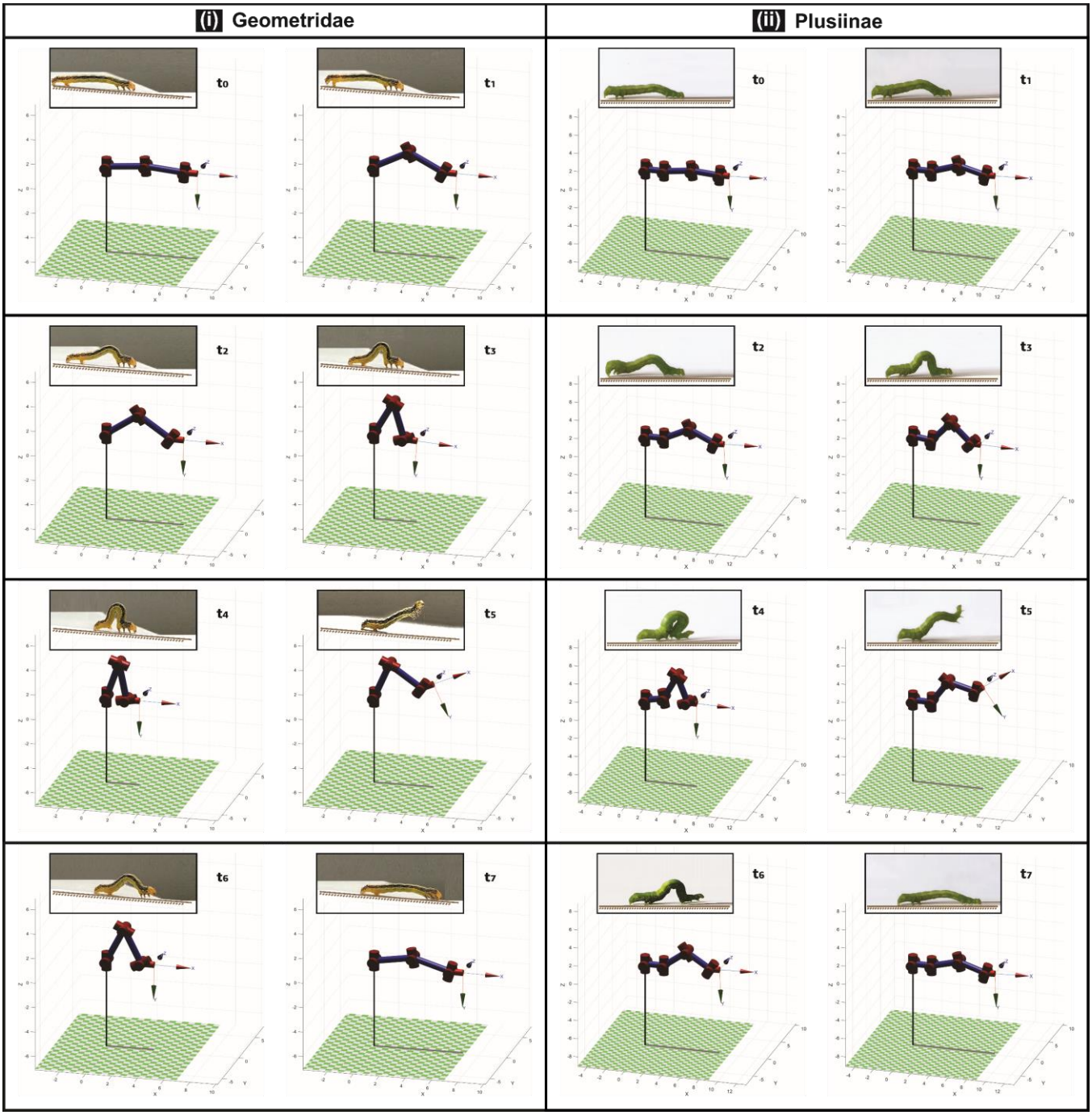

Figure 13. 3-D Kinematic Chain modeled in Matlab® for (i) *Geometridae* and (ii) *Plusiinae* caterpillars

Appendix 1

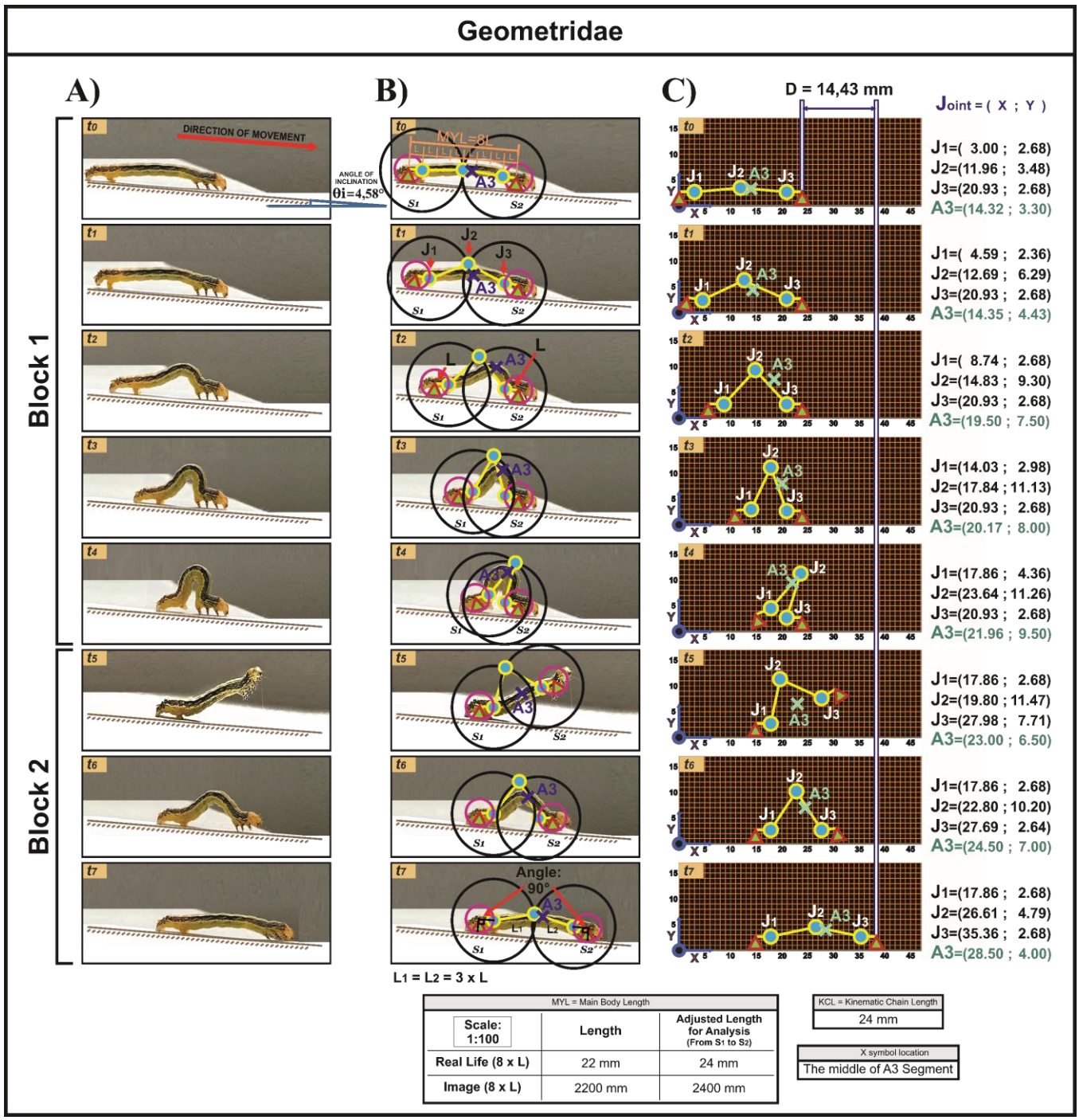

Figure A.1. Kinematic Chain Definition on *Geometridae* by the application of the GEKINS. Columns: A) Insect during Inching-Locomotion in 8 (t_0-t_7) Phases of Walk-Stride (PHAWS). B) Location of the Attachment Mechanisms-Suction Cups (S_1 and S_2), Joints (J_1, J_2 and J_3), and Links (L, L_1 and L_2). C) Joint Location on Grid Graphics in scale 1:100, and WSL. Note that t_0-t_7 represents PHAWS. Note that X symbol means the location of the middle at A3 anatomical segment.

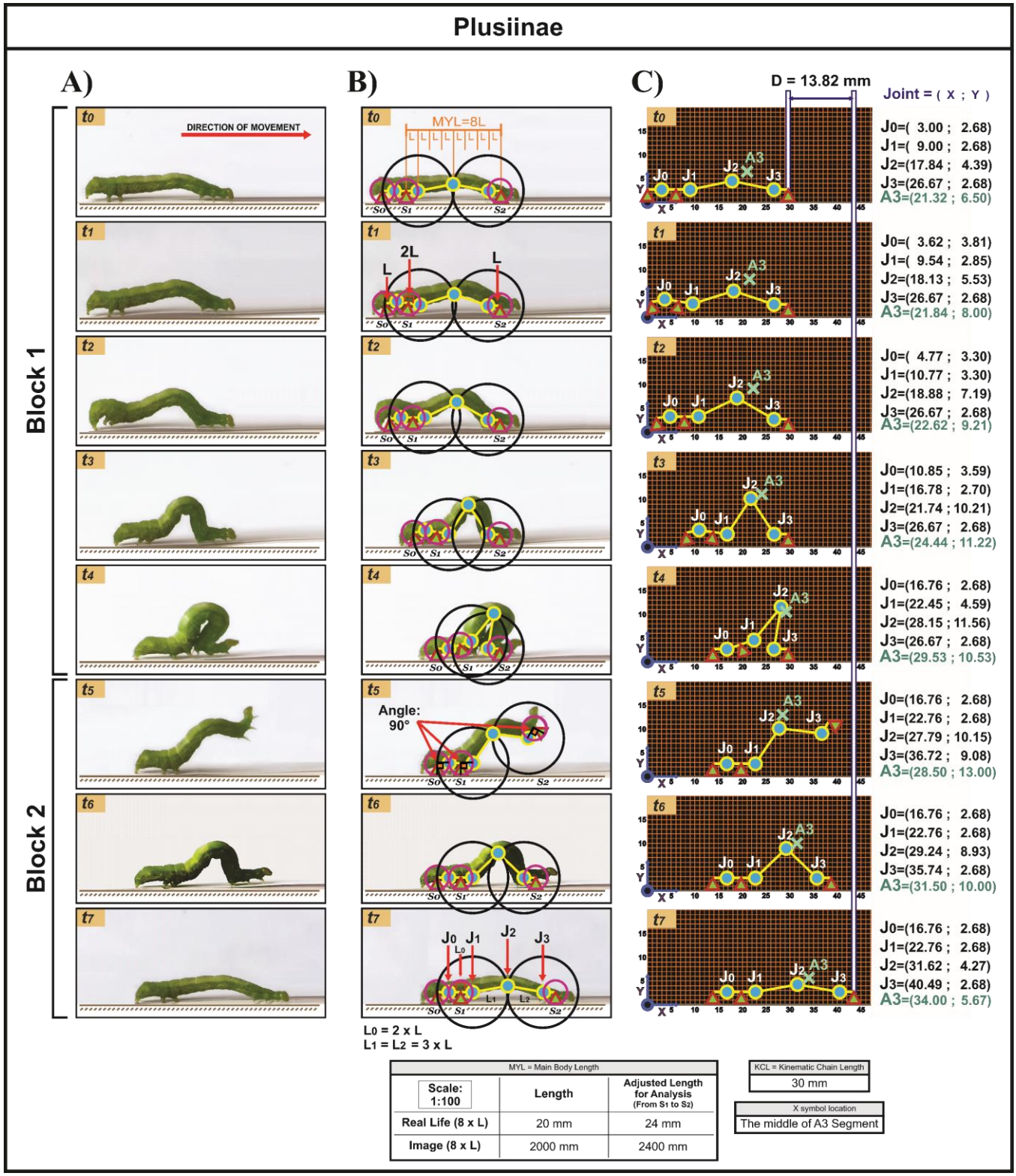

Figure A.2. Kinematic Chains Definition on *Plusiinae* by the application of the GEKINS. Columns: A) Insect during Inching-Locomotion in 8 (t_0-t_7) Phases of Walk-Stride (PHAWS). B) Location of the Attachment Mechanisms-Suction Cups (S_0, S_1 S_2), Joints (J_0, J_1, J_2 and J_3), and Links (L, L_0, L_1 and L_2). C) Joint Location on Grid Graphics in scale 1:100, and WSL. Note that t_0-t_7 represents PHAWS. Note that X symbol means the location at the middle of A3 anatomical segment.

Appendix 2

Table A. GEKINS Algorithm

Inputs	PHAWS photograms	
GEKINS Steps	1	Attachment Mechanism Location, placing the Suction Cups (*S*)
	2	Define MYL: the distance between Suction Cup (*S*) 1 to 2
	3	Lateral Joint (J_L) Location, placing the DOF using a lateral view
	4	Draw Links (Li), connect the joints with rigid lines
	5	Top Joint (J_T) Location, placing the DOF using a top view
	6	D-H convention
Outputs	A	End-effector (Caterpillar's head) position
	B	Joint angle's behavior : "angular displacement (θ) / average velocity (ω)"

Appendix 3

Table B. Joint Location in X-Y axis by PHAWS for *Geometridae* and *Plusiinae*

Caterpillar	**Ji**	**Location (mm)**	**PHAWS**							
			t_0	**t_1**	**t_2**	**t_3**	**t_4**	**t_5**	**t_6**	**t_7**
Geometridae	**J_0**	X	-	-	-	-	-	-	-	-
		Y	-	-	-	-	-	-	-	-
Plusiinae		X	0.00	0.62	1.77	7.85	13.76	13.76	13.76	13.76
		Y	0.00	1.13	0.62	0.91	0.00	0.00	0.00	0.00
Geometridae	**J_1**	X	0.00	1.59	5.74	11.03	14.86	14.86	14.86	14.86
		Y	0.00	-0.32	0.00	0.30	1.68	0.00	0.00	0.00
Plusiinae		X	0.00	0.54	1.77	7.78	13.45	13.76	13.76	13.76
		Y	0.00	0.17	0.62	0.02	1.91	0.00	0.00	0.00
Geometridae	**J_2**	X	0.00	0.72	2.87	5.88	11.68	7.84	10.84	14.65
		Y	0.00	2.81	5.82	7.65	7.78	7.99	6.72	1.31
Plusiinae		X	0.00	0.30	1.05	3.91	10.32	9.95	11.41	13.79
		Y	0.00	1.13	2.80	5.82	7.17	5.76	4.54	-0.13
Geometridae	**J_3**	X	0.00	0.00	0.00	0.00	0.00	7.05	6.76	14.43
		Y	0.00	0.00	0.00	0.00	0.00	5.03	-0.04	0.00
Plusiinae		X	0.00	0.00	0.00	0.00	0.00	10.05	9.07	13.82
		Y	0.00	0.00	0.00	0.00	0.00	6.40	0.00	0.00

Appendix 4

Table C. D-H Parameters of Locomotion - Sequence H-T (2-D). *Geometridae* and *Plusiinae*

	Geometridae					***Plusiinae***			
Link $_i$	***θ_i***	***d_i***	***a_i***	***α_i***		***θ_i***	***d_i***	***a_i***	***α_i***
1	θ_3	0	L_2 = 3 x "L"	0		θ_3	0	L_2 = 3 x "L"	0
2	θ_2	0	L_1 = 3 x "L"	0		θ_2	0	L_1 = 3 x "L"	0
3	θ_1	0	L	0		θ_1	0	L_o = 2 x "L"	0
4	-	-	-	-		θ_0	0	L	0

Appendix 5

Table D. D-H Parameters of Locomotion - Sequence T-H (2-D). *Geometridae* and *Plusiinae*

Link $_i$	***Geometridae***					***Plusiinae***			
	θ_i	***d_i***	***a_i***	***α_i***		***θ_i***	***d_i***	***a_i***	***α_i***
1	θ_1	0	L_1 = 3 x "L"	0		θ_0	0	L_o = 2 x "L"	0
2	θ_2	0	L_2 = 3 x "L"	0		θ_1	0	L_1 = 3 x "L"	0
3	θ_3	0	L = "L"	0		θ_2	0	L_2 = 3 x "L"	0
4	-	-	-	-		θ_3	0	L	0

Appendix 6

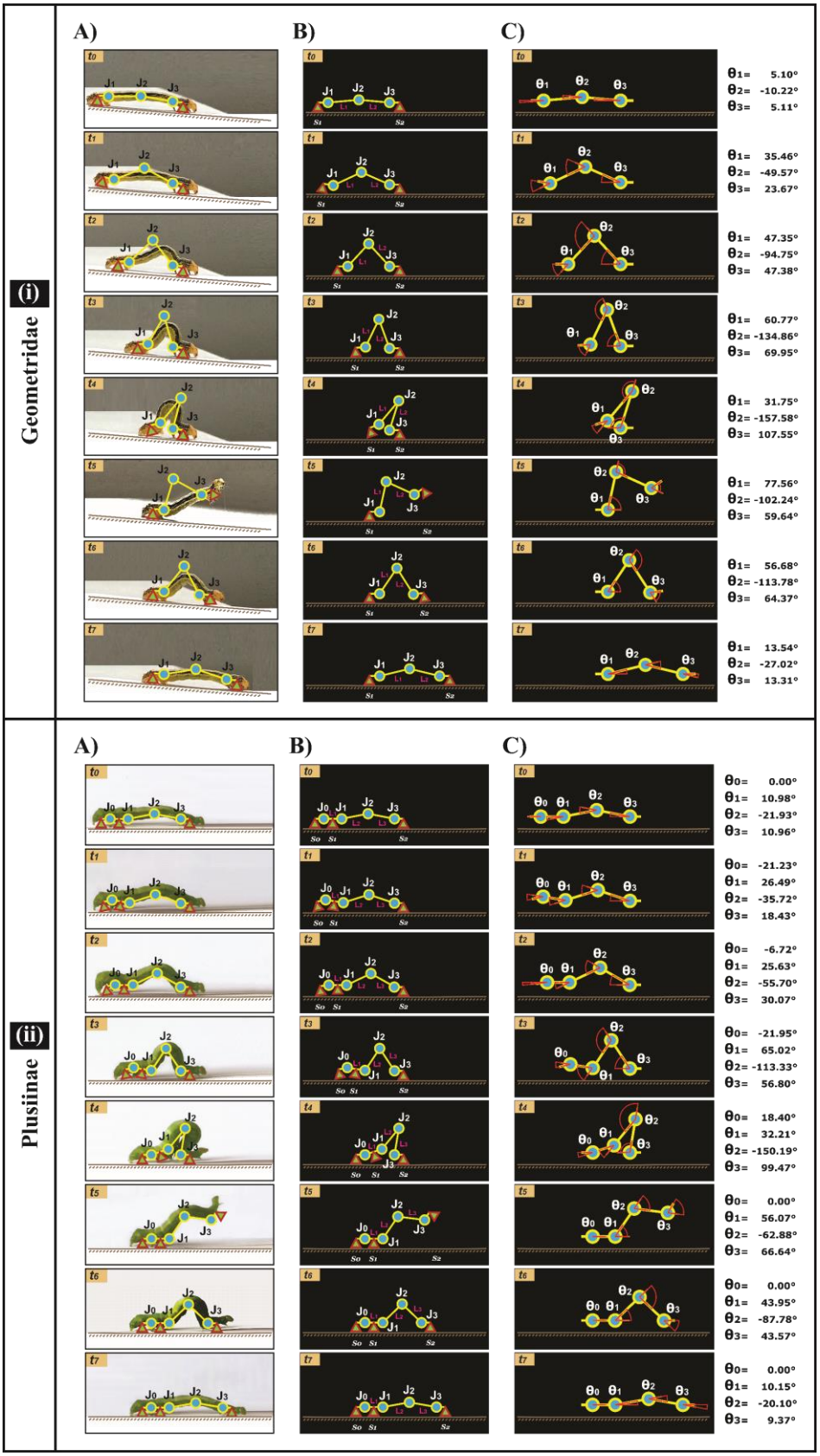

Figure B. Joint's angular displacement on (i) *Geometridae* and (ii) *Plusiinae*. Columns: A) Insect and kinematic chain during inching-locomotion in 8 phases. B) Kinematic chain locomotion. C) Angular displacement in degrees by each Joint. Note that t_0-t_7 represents PHAWS.

Appendix 7

Table E. Angular displacement by PHAWS

Caterpillar	θ_i (°)	PHAWS							
		t_0	t_1	t_2	t_3	t_4	t_5	t_6	t_7
Geometridae	θ_0	-	-	-	-	-	-	-	-
Plusiinae	θ_0	0.00	-21.23	-6.72	-21.95	18.40	0.00	0.00	0.00
Geometridae	θ_1	5.10	35.46	47.35	60.77	31.75	77.56	56.68	13.54
Plusiinae	θ_1	10.98	26.49	25.63	65.02	32.21	56.07	43.95	10.15
Geometridae	θ_2	-10.22	-49.57	-94.75	-134.86	-157.58	-102.24	-113.78	-27.02
Plusiinae	θ_2	-21.93	-35.72	-55.70	-113.33	-150.19	-62.88	-87.78	-20.10
Geometridae	θ_3	5.11	23.67	47.38	69.95	107.55	59.64	64.37	13.31
Plusiinae	θ_3	10.96	18.43	30.07	56.80	99.47	66.64	43.57	9.37

Appendix 8

Table F. Equations of Joint Angle's Behavior by PHAWS – *Geometridae* and *Plusiinae*

Caterpillar	Ji	Joint Angle's Behavior	PHAWS						
			$t_0 - t_1$	$t_1 - t_2$	$t_2 - t_3$	$t_3 - t_4$	$t_4 - t_5$	$t_5 - t_6$	$t_6 - t_7$
			$0 \leq t < 1$	$1 \leq t < 2$	$2 \leq t < 3$	$3 \leq t < 4$	$4 \leq t < 5$	$5 \leq t < 6$	$6 \leq t \leq 7$
Geometridae	J_0	θ_0 (°)	-	-	-	-	-	-	-
		ω_0 (°/s)	-	-	-	-	-	-	-
Plusiinae	J_0	θ_0 (°)	-21.23t	14.51t -35.74	-15.23t + 23.74	40.35t – 143	-18.40t + 92	0	0
		ω_0 (°/s)	-21.23	14.51	-15.23	40.35	-18.40	0	0
Geometridae	J_1	θ_1 (°)	30.36t + 5.1	11.89t + 23.57	13.42t + 20.51	-29.02t + 147.83	45.81t – 151.49	-20.88t + 181.96	-43.14t + 315.52
		ω_1 (°/s)	30.36	11.89	13.42	-29.02	45.81	-20.88	-43.14
Plusiinae	J_1	θ_1 (°)	15.51t + 10.98	-0.86t + 27.35	39.39t – 53.15	-32.81t + 163.45	23.86t – 63.23	-12.12t + 116.67	-33.80t + 246.75
		ω_1 (°/s)	15.51	-0.86	39.39	-32.81	23.86	-12.12	-33.80
Geometridae	J_2	θ_2 (°)	-39.35t – 10.22	-45.18t – 4.39	-40.11t – 14.53	-22.72t – 66.7	55.34t – 378.94	-11.54t – 44.54	86.76t – 634.34
		ω_2 (°/s)	-39.35	-45.18	-40.11	-22.72	55.34	-11.54	86.76
Plusiinae	J_2	θ_2 (°)	-13.79t – 21.93	-19.98t – 15.74	-57.63t + 59.56	-36.86t – 2.75	87.31t – 499.43	-24.90t + 61.62	67.68t – 493.86
		ω_2 (°/s)	-13.79	-19.98	-57.63	-36.86	87.31	-24.90	67.68
Geometridae	J_3	θ_3 (°)	18.56t + 5.11	23.71t – 0.04	22.57t – 2.24	37.60t – 42.85	-47.91t + 299.19	4.73t + 35.99	-51.06t + 370.73
		ω_3 (°/s)	18.56	23.71	22.57	37.60	-47.91	4.73	-51.06
Plusiinae	J_3	θ_3 (°)	7.47t + 10.96	11.64t + 6.79	26.73t – 23.39	42.67t – 71.21	-32.83t + 230.79	-23.07t + 181.99	-34.20t + 248.77
		ω_3 (°/s)	7.47	11.64	26.73	42.67	-32.83	-23.07	-34.20

Appendix 9

Table G. D-H Parameters of Locomotion (3-D). *Geometridae* and *Plusiinae*

Link $_i$	*Geometridae*								*Plusiinae*							
	Sequence H-T				Sequence T-H				Sequence H-T				Sequence T-H			
	θ_i	d_i	a_i	α_i	θ_i	d_i	a_i	α_i	θ_i	d_i	a_i	α_i	θ_i	d_i	a_i	α_i
1	θ_{T3}	0	0	- π /2	θ_{T1}	0	0	π /2	θ_{T3}	0	0	- π /2	θ_{T0}	0	0	π /2
2	θ_3	L_{T2}	L_2	π /2	θ_1	$-L_{T1}$	L_1	-π /2	θ_3	L_{T2}	L_2	π /2	θ_0	$-L_{T0}$	L_0	-π /2
3	θ_{T2}	0	0	- π /2	θ_{T2}	0	0	π /2	θ_{T2}	0	0	- π /2	θ_{T1}	0	0	π /2
4	θ_2	L_{T1}	L_1	π /2	θ_2	$-L_{T2}$	L_2	-π /2	θ_2	L_{T1}	L_1	π /2	θ_1	$-L_{T1}$	L_1	-π /2
5	θ_{T1}	0	0	- π /2	θ_{T3}	0	0	π /2	θ_{T1}	0	0	- π /2	θ_{T2}	0	0	π /2
6	θ_1	0	L	0	θ_3	0	L	0	θ_1	L_{T0}	L_0	π /2	θ_2	$-L_{T2}$	L_2	-π /2
7	-	-	-	-	-	-	-	-	θ_{T0}	0	0	- π /2	θ_{T3}	0	0	π /2
8	-	-	-	-	-	-	-	-	θ_0	0	L	0	θ_3	0	L	0

Appendix 10

Table H. Matlab® Implementation of Kinematic Chains in 3 Dimensions – *Geometridae* and *Plusiinae*

Steps	***Geometridae***		***Plusiinae***
1	Link Dimensions % Adapted to the values used in GEKINS		
	L_1=3; LT1=0; L_2=3; LT2=0; L=1;		LT0=0; L_0=2; LT1=0; L_1=3; LT2=0; L_2=3; L=1;
2	D-H Parameters		
2.1	Sequence H-T Locomotion:		
	L_HT(1)=Link([0 0 0 -pi/2]); L_HT(2)=Link([0 LT2 L_2 pi/2]); L_HT(3)=Link([0 0 0 -pi/2]); L_HT(4)=Link([0 LT1 L_1 pi/2]); L_HT(5)=Link([0 0 0 -pi/2]); L_HT(6)=Link([0 0 L 0]);		L_HT(1)=Link([0 0 0 -pi/2]); L_HT(2)=Link([0 LT2 L_2 pi/2]); L_HT(3)=Link([0 0 0 -pi/2]); L_HT(4)=Link([0 LT1 L_1 pi/2]); L_HT(5)=Link([0 0 0 -pi/2]); L_HT(6)=Link([0 LT0 L_0 0]); L_HT(7)=Link([0 0 0 0]); L_HT(8)=Link([0 0 L 0]);
2.2	Sequence T-H Locomotion:		
	L_TH(1)=Link([0 0 0 -pi/2]); L_TH(2)=Link([0 LT1 L_1 pi/2]); L_TH(3)=Link([0 0 0 -pi/2]); L_TH(4)=Link([0 LT2 L_2 pi/2]); L_TH(5)=Link([0 0 0 -pi/2]); L_TH(6)=Link([0 0 L 0]);		L_TH(1)=Link([0 0 0 -pi/2]); L_TH(2)=Link([0 LT0 L_0 pi/2]); L_TH(3)=Link([0 0 0 -pi/2]); L_TH(4)=Link([0 LT1 L_1 pi/2]); L_TH(5)=Link([0 0 0 -pi/2]); L_TH(6)=Link([0 LT2 L_2 0 pi/2]); L_TH(7)=Link([0 0 0 -pi/2]); L_TH(8)=Link([0 0 L 0]);
3	Join all Links:		
	Insect1_HT=SerialLink(L_HT); Insect1_TH=SerialLink(L_TH);		Insect2_HT=SerialLink(L_HT); Insect2_TH=SerialLink(L_TH);
4	Kinematic Chain Display:		
	Insect1_HT.name='Geometridae Kinematic Chain'; Insect1_HT.plot([0 0 0 0 0 0]) Insect1_TH.name='Geometridae Kinematic Chain'; Insect1_TH.plot([0 0 0 0 0 0])		Insect2_HT.name='Plusiinae Kinematic Chain'; Insect2_HT.plot([0 0 0 0 0 0 0 0]) Insect2_TH.name='Plusiinae Kinematic Chain'; Insect2_TH.plot([0 0 0 0 0 0 0 0])

Appendix 11

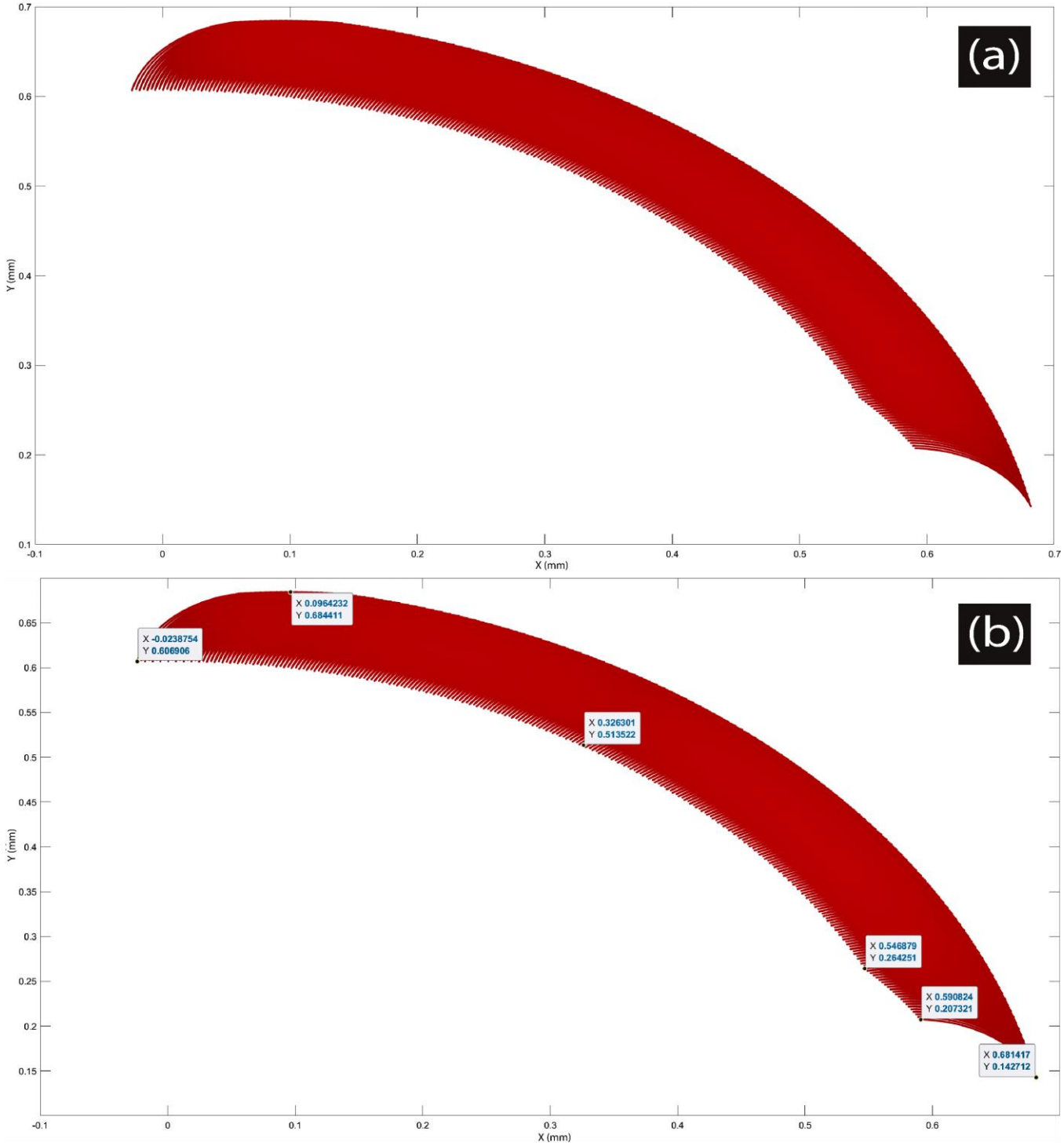

Figure C.1. Planar Workspace of *Geometridae*'s Kinematic Chain. a) Red surface, b) Selected points.

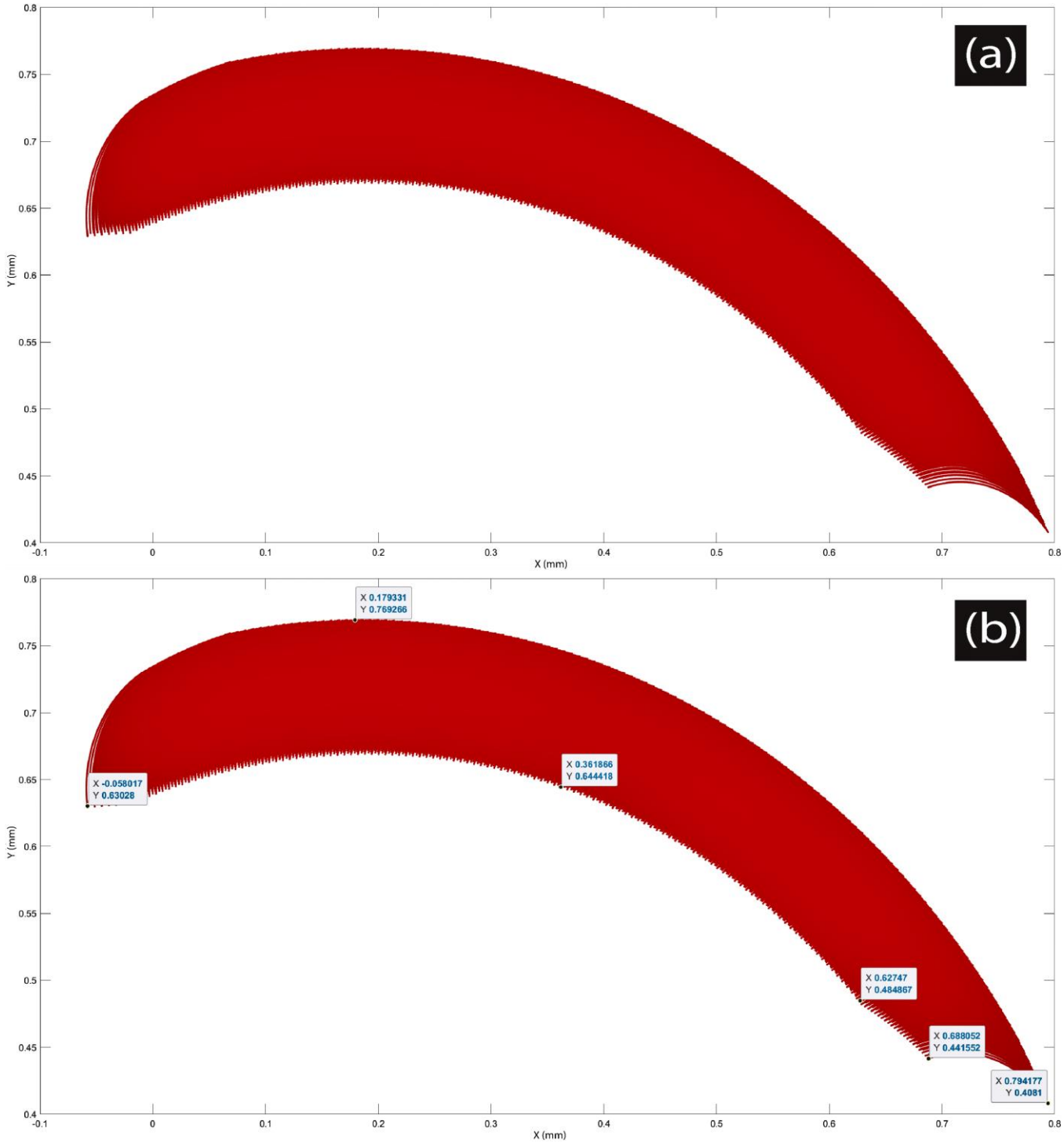

Figure C.2. Planar Workspace of *Plusiinae*'s Kinematic Chain. a) Red surface, b) Selected points.

Appendix 12

Table I. Matlab® Implementation of Kinematic Chain's Workspace in 2 Dimensions – *Geometridae* and *Plusiinae*

Steps	***Geometridae***		***Plusiinae***
1	Link Dimensions % The proportional length (given in milimeters) is based on GEKINS algorithm.		
	L_1=0.3; L_2=0.3; L3=0.1;		L_0=0.2; L_1=0.3; L_2=0.3; L3=0.1;
2	D-H Parameters		
	L(1)= Link([0 0 L_1 0]); L(2)= Link([0 0 L_2 0]); L(3)= Link([0 0 L3 0]);		L(1)= Link([0 0 L_0 0]); L(2)= Link([0 0 L_1 0]); L(3)= Link([0 0 L_2 0]); L(4)= Link([0 0 L3 0]);
3	Angle definition		

	th1 = (0.029*pi:0.01:0.4*pi) ;
	th2 = (0.057*pi:0.01:0.126*pi);
	th3 = (0.029*pi:0.01:0.406*pi) ;
	q = {th1,th2,th3};
			th1 = (0.10*pi:0.01:0.122*pi);
			th2 = (0.029*pi:0.01:0.4*pi);
			th3 = (0.057*pi:0.01:0.126*pi);
			th4 = (0.029*pi:0.01:0.406*pi) ;
			q = {th1,th2,th3,th4};

4	Preliminary coding for data display		

	r = SerialLink(L);
	r.display()
	[~,n] = size(L);
	
	var = sym('q',[n 1]);
	assume(var,'real')		

5	Workspace Generation		

	[Q{1:numel(q)}] = ndgrid(q{:});
	T = simplify(vpa(r.fkine(var),3));
	Pos = T.tv;
	x(var(:)) = Pos(1);
	X = matlabFunction(x);
	X = X(Q{:});
	y(var(:)) = Pos(2);
	Y = matlabFunction(y);
	Y = Y(Q{:});
	plot(X(:),Y(:),'r.')
	xlabel('X')
	ylabel('Y')		

Appendix 13

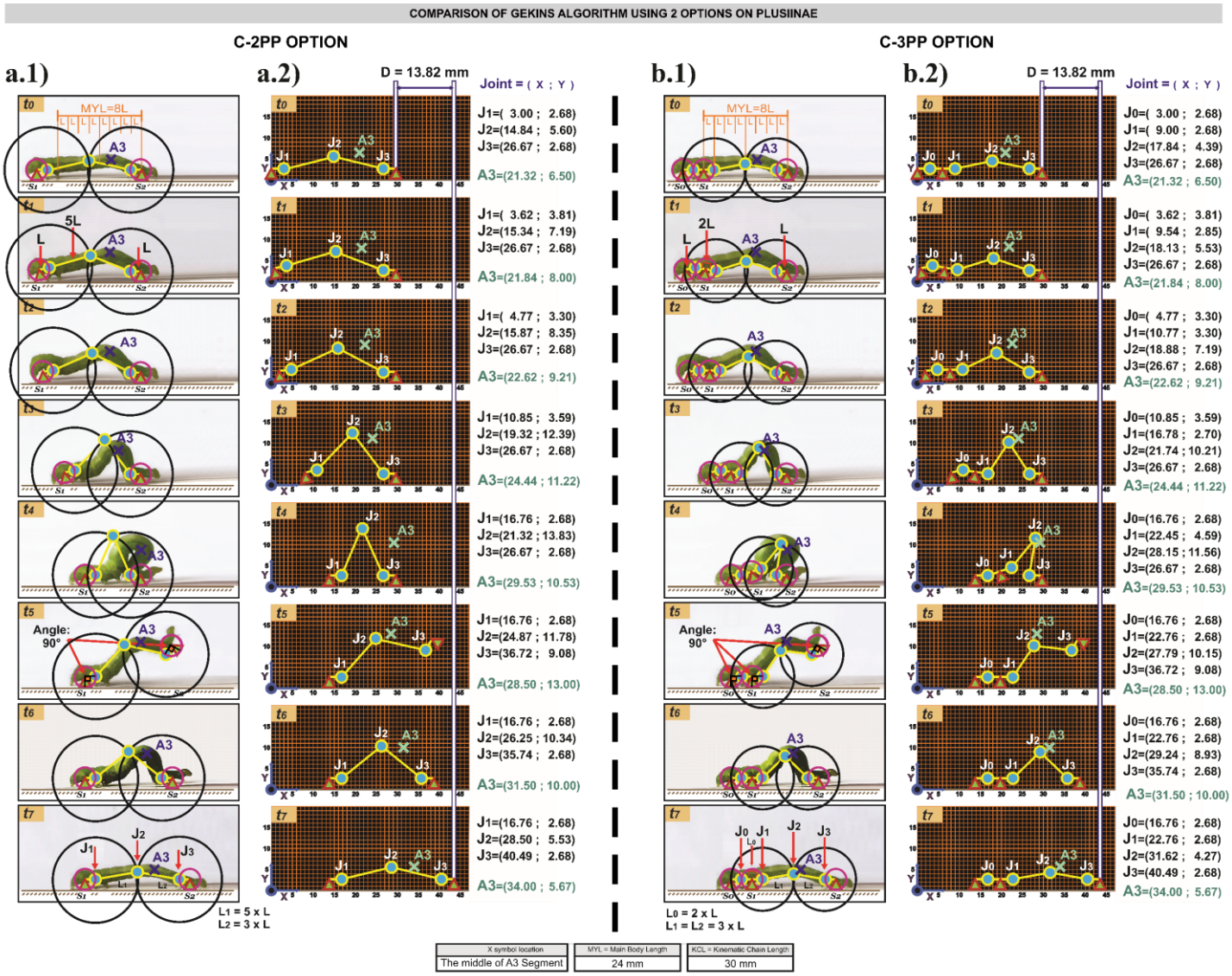

Figure D. Checking GEKINS algorithm using 2 options on *Plusiinae* Kinematic Chain modeling: C-3PP and C-2PP. Note that with the use of C-2PP, the S_0, J_0, and L_0 were not taken into account due to the pair of prolegs located in the A5 segment had been hidden. The results show that the better accurate option is C-3PP, because it depicts the minimum distance ($D_{J2\text{-}A3}$) between J_2 - A3 anatomical segment for each PHAWS. a.1 and b.1) Location of the Attachment Mechanisms-Suction Cups (S_1 S_2), Joints (J_1, J_2 and J_3), and Links (L, L_1 and L_2); a.2 and b.2) Joint Location on Grid Graphics in scale 1:100, and WSL. The closer those parameters (J_2 - A3) are located, the more accurate the model is.

Table J. Error Distance between J_2 – A3 in mm

PHAWS	Validation of GEKINS Algorithm on *Plusiinae*		
	Using C-2PP Option	Using C-3PP Option	Distance reduction
t_0	6.54	4.07	37,8%
t_1	6.55	4.46	31,9%
t_2	6.80	4.25	37,5%
t_3	5.25	2.88	45,1%
t_4	8.83	1.69	80,9%
t_5	3.83	2.94	23,2%
t_6	5.26	2.50	52,5%
t_7	5.50	2.76	49,8%
Average	**6.07**	**3.19**	**47,4%**

References

[1] D. M. Wilson, "Insect Walking," *Annual Review of Entomology*, vol. 11, no. 1, pp. 103-122, 1966, doi: 10.1146/annurev.en.11.010166.000535.

[2] T. Cornelissen, F. Cintra, and J. C. Santos, "Shelter-Building Insects and Their Role as Ecosystem Engineers," *Neotropical Entomology*, vol. 45, no. 1, pp. 1-12, 2016/02/01 2016, doi: 10.1007/s13744-015-0348-8.

[3] A. Humeau, M. Piñeirua, J. Crassous, and J. Casas, "Locomotion of Ants Walking up Slippery Slopes of Granular Materials," (in eng), *Integr Org Biol*, vol. 1, no. 1, p. obz020, 2019, doi: 10.1093/iob/obz020.

[4] H. Cruse, V. Dürr, M. Schilling, and J. Schmitz, "Principles of Insect Locomotion," in *Spatial Temporal Patterns for Action-Oriented Perception in Roving Robots*, P. Arena and L. Patanè Eds. Berlin, Heidelberg: Springer Berlin Heidelberg, 2009, pp. 43-96.

[5] M. Zimmer, "Insect locomotion: Flies show you how to stay on course," *Current Biology*, vol. 31, no. 20, pp. R1395-R1397, 2021/10/25/ 2021, doi: https://doi.org/10.1016/j.cub.2021.09.015.

[6] T. Ireland and S. Garnier, "Architecture, space and information in constructions built by humans and social insects: a conceptual review," *Philosophical Transactions of the Royal Society B: Biological Sciences*, vol. 373, no. 1753, p. 20170244, 2018, doi: doi:10.1098/rstb.2017.0244.

[7] L. M. Theunissen, H. H. Bekemeier, and V. Dürr, "On the natural statistics of insect locomotion: indications for two distinct mechanisms of step generation," in *Front Behav Neurosci Conference Abstract: Tenth International Congress of Neuroethology. doi: 10.3389/conf. fnbeh*, 2012, vol. 150.

[8] S. S. Bidaye, T. Bockemühl, and A. Büschges, "Six-legged walking in insects: how CPGs, peripheral feedback, and descending signals generate coordinated and adaptive motor rhythms," *Journal of Neurophysiology*, vol. 119, no. 2, pp. 459-475, 2018, doi: 10.1152/jn.00658.2017.

[9] L. Chittka and N. Rossi, "Social cognition in insects," *Trends in Cognitive Sciences*, vol. 26, no. 7, pp. 578-592, 2022/07/01/ 2022, doi: https://doi.org/10.1016/j.tics.2022.04.001.

[10] L. Wang *et al.*, "Symbiotic human-robot collaborative assembly," *CIRP Annals*, vol. 68, no. 2, pp. 701-726, 2019/01/01/ 2019, doi: https://doi.org/10.1016/j.cirp.2019.05.002.

[11] A. Nemiroski *et al.*, "Arthrobots," *Soft robotics*, vol. 4, no. 3, pp. 183-190, 2017.

[12] P. Ramdya *et al.*, "Climbing favours the tripod gait over alternative faster insect gaits," *Nature Communications*, vol. 8, no. 1, p. 14494, 2017/02/17 2017, doi: 10.1038/ncomms14494.

[13] R. Kukillaya, J. Proctor, and P. Holmes, "Neuromechanical models for insect locomotion: Stability, maneuverability, and proprioceptive feedback," *Chaos: An Interdisciplinary Journal of Nonlinear Science*, vol. 19, no. 2, p. 026107, 2009, doi: 10.1063/1.3141306.

[14] D. E. Koditschek, R. J. Full, and M. Buehler, "Mechanical aspects of legged locomotion control," (in eng), *Arthropod Struct Dev*, vol. 33, no. 3, pp. 251-72, Jul 2004, doi: 10.1016/j.asd.2004.06.003.

[15] J. R. Serres and F. Ruffier, "Optic flow-based collision-free strategies: From insects to robots," *Arthropod Structure & Development*, vol. 46, no. 5, pp. 703-717, 2017/09/01/ 2017, doi: https://doi.org/10.1016/j.asd.2017.06.003.

[16] J. Cornejo *et al.*, "Industrial, collaborative and mobile robotics in Latin America: Review of mechatronic technologies for advanced automation," *Emerg. Sci. J.*, vol. 7, no. 4, pp. 1430-1458, 2023 2023, doi: 10.28991/esj-2023-07-04-025.

[17] C. Pinciroli *et al.*, "Swarm Construction: A Method in Multi-Agent Robotic Assembly," *Worcester Polytechnic Institute*, 2020.

[18] P. Manoonpong *et al.*, "Insect-inspired robots: Bridging biological and artificial systems," *Sensors*, vol. 21, no. 22, p. 7609, 2021.

[19] H. B. Brown, M. Friedman, Y. Xu, and T. Kanade, "Self mobile space manipulator project," in *5th Annual Workshop on Space Operations Applications and Research (SOAR 1991)*, 1992, vol. 1, p. 362.

[20] M. H. Dickinson, "Bionics: Biological insight into mechanical design," *Proceedings of the National Academy of Sciences*, vol. 96, no. 25, pp. 14208-14209, 1999, doi: doi:10.1073/pnas.96.25.14208.

[21] G. C. H. E. de Croon, J. J. G. Dupeyroux, S. B. Fuller, and J. A. R. Marshall, "Insect-inspired AI for autonomous robots," *Science Robotics*, vol. 7, no. 67, p. eabl6334, 2022, doi: doi:10.1126/scirobotics.abl6334.

[22] NCBI, "Taxonomy browser (Geometridae)," 2023. Accessed: 2023/3/1. [Online]. Available: https://www.ncbi.nlm.nih.gov/Taxonomy/Browser/wwwtax.cgi?mode=Info&id=82593&lvl=3&lin=f&keep=1&srchmode=1&unlock

[23] A. Hausmann, "The Geometrid Moths of Europe," ed: Brill, 2001.

[24] BugGuide, "Family Geometridae - Geometrid Moths." Accessed: 2022/12/26. [Online]. Available: https://bugguide.net/node/view/188/data

[25] A. Lindt and J. Viidalepp, "Oospila bulava, a new emerald geometrid moth from South America (Lepidoptera, Geometridae, Geometrinae),"

Zootaxa, vol. 4058, no. 1, pp. 142-144, 2015 2015, doi: 10.11646/zootaxa.4058.1.11.

[26] I. Kostjuk, V. G. Mironov, and J. Viidalepp, "Review of the Central Asian species of Phthorarcha Meyrick (Geometridae: Alsophilinae) with description of a new species," *Zootaxa*, vol. 4861, no. 2, p. zootaxa.4861.2.4, 2020 2020, doi: 10.11646/zootaxa.4861.2.4.

[27] NCBI, "Taxonomy browser (Plusiinae)," 2023. Accessed: 2023/3/1. [Online]. Available: https://www.ncbi.nlm.nih.gov/Taxonomy/Browser/wwwtax.cgi?mode=Info&id=95186&lvl=3&lin=f&keep=1&srchmode=1&unlock

[28] M. Sajjad *et al.*, "First record and taxonomic description of the genus Thysanoplusia (Fabricius) (Lepidoptera: Noctuidae: Plusiinae) from Pakistan," *Saudi Journal of Biological Sciences*, vol. 27, no. 5, pp. 1375-1379, 2020/05/01/ 2020, doi: https://doi.org/10.1016/j.sjbs.2019.12.006.

[29] T. D. Eichlin, H. B. Cunningham, T. D. Eichlin, and H. B. Cunningham, "The plusiinae (Lepidoptera: Noctuidae) of America north of Mexico, emphasizing genitalic and larval morphology," 1978 1978, doi: 10.22004/AG.ECON.158098.

[30] BugGuide, "Subfamily Plusiinae - Looper Moths." Accessed: 2022/12/26. [Online]. Available: https://bugguide.net/node/view/12377/data

[31] I. Chou, "Studies on Chinese Plusiinae (Lepidoptera: Noctuidae)," *Acta Entomol. Sinica*, vol. 17, pp. 66-82, 1974.

[32] V. Kravchenko *et al.*, "The Plusiinae of Israel (Lepidoptera: Noctuidae)," *SHILAP Revista de lepidopterología*, vol. 33, no. 132, pp. 449-459, 2005.

[33] A. Ghanbari, A. Rostami, S. M. R. S. Noorani, and M. M. S. Fakhrabadi, "Modeling and simulation of inchworm mode locomotion," in *International conference on intelligent robotics and applications*, 2008: Springer, pp. 617-624.

[34] W. Wei, W. Yingying, W. Kun, Z. Houxiang, and Z. Jianwei, "Analysis of the kinematics of module climbing caterpillar robots," in *2008 IEEE/ASME International Conference on Advanced Intelligent Mechatronics*, 2-5 July 2008 2008, pp. 84-89, doi: 10.1109/AIM.2008.4601639.

[35] W. Wang, K. Wang, and H. Zhang, "Crawling gait realization of the mini-modular climbing caterpillar robot," *Progress in Natural Science*, vol. 19, no. 12, pp. 1821-1829, 2009/12/10/ 2009, doi: https://doi.org/10.1016/j.pnsc.2009.07.009.

[36] H. B. B. a. M. F. a. T. K. a. Y. Xu, C.-M. U. R. Institute, Ed. *Self Mobile Space Manipulator Project*. Annual Research Review, 1990.

[37] M. H. Nair, M. C. Rai, and M. Poozhiyil, "Design engineering a walking robotic manipulator for in-space assembly missions," *Frontiers in Robotics and AI*, p. 277, 2022.

[38] Y. Jin, J. Li, S. Liu, G. Cao, and J. Liu, "A worm-inspired robot based on origami structures driven by the magnetic field," *Bioinspiration & Biomimetics*, vol. 18, no. 4, p. 046008, 2023/05/24 2023, doi: 10.1088/1748-3190/acd59e.

[39] S. Sponberg, "animal locomotion," *Physics Today*, vol. 70, pp. 9-34, 2017.

[40] K. Karakasiliotis *et al.*, "From cineradiography to biorobots: an approach for designing robots to emulate and study animal locomotion," *Journal of The Royal Society Interface*, vol. 13, no. 119, p. 20151089, 2016.

[41] A. Biewener and S. Patek, *Animal locomotion*. Oxford University Press, 2018.

[42] H. Cruse, V. Dürr, M. Schilling, and J. Schmitz, "Principles of insect locomotion," *Spatial temporal patterns for action-oriented perception in roving robots*, pp. 43-96, 2009.

[43] R. J. Marquis and S. Koptur, "Synopsis and the Future of Caterpillar Research," in *Caterpillars in the Middle: Tritrophic Interactions in a Changing World*, R. J. Marquis and S. Koptur Eds. Cham: Springer International Publishing, 2022, pp. 609-622.

[44] I. F. B. Common, *Moths of Australia / I.F.B. Common ; with photographs by Ederic Slater* (no. Accessed from https://nla.gov.au/nla.cat-vn183973). Carlton, Vic: Melbourne University Press, 1990.

[45] F. W. Stehr, "Immature Insects. Kendall," ed: Hunt Publishing Company, Dubuque, Iowa, USA, 1987.

[46] P. A. Opler, *Peterson first guide to butterflies and moths*. Houghton Mifflin Harcourt, 1998.

[47] C. T. Maier, *Caterpillars on the foliage of conifers in the Northeastern United States*. USDA Forest Service, Forest Health Technology Enterprise Team, 2004.

[48] P. Corke, *Robotics, Vision and Control*. Cham: Springer International Publishing, 2017.

[49] M. L. Zelditch, D. L. Swiderski, and H. D. Sheets, *Geometric morphometrics for biologists: a primer*. academic press, 2012.

[50] ISO, "Iso/Tc 266 Biomimetics," 2023 2023. [Online]. Available: https://www.iso.org/committee/652577.html.

[51] Y. Bar-Cohen, *Biomimetics: nature-based innovation*. CRC press, 2011.

[52] H. Rajabi, J. Wu, and S. Gorb, "Insects: Functional Morphology, Biomechanics and Biomimetics," *Insects*, vol. 12, no. 12, p. 1108, 2021. [Online]. Available: https://www.mdpi.com/2075-4450/12/12/1108.

[53] U. o. Guelph. "Bio-Inspired Design (BID) Community- Center for Biologically Inspired Design." https://bioinspired.sinet.ca/ (accessed.

[54] N. Pentelovitch and J. K. Nagel, "Understanding the Use of Bio-Inspired Design Tools by Industry Professionals," *Biomimetics*, vol. 7, no. 2, p. 63,

2022. [Online]. Available: https://www.mdpi.com/2313-7673/7/2/63.
[55] D. Brady, A. Saviane, S. Cappellozza, and F. Sandrelli, "The Circadian Clock in Lepidoptera," (in eng), *Front Physiol*, vol. 12, p. 776826, 2021, doi: 10.3389/fphys.2021.776826.
[56] E. S. Fortune and N. J. Cowan, "Robot Behavior," in *Encyclopedia of Animal Behavior*, M. D. Breed and J. Moore Eds. Oxford: Academic Press, 2010, pp. 87-90.
[57] M. Tamborini, "The elephant in the room: The biomimetic principle in bio-robotics and embodied AI," *Studies in History and Philosophy of Science*, vol. 97, pp. 13-19, 2023/02/01/ 2023, doi: https://doi.org/10.1016/j.shpsa.2022.11.007.
[58] Mathworks. "Build manipulator robot using kinematic DH parameters - MATLAB & Simulink." https://www.mathworks.com/help/robotics/ug/build-manipulator-robot-using-kinematic-dh-parameters.html (accessed.
[59] P. Corke, W. Jachimczyk, and R. Pillat, "Robot Arm Kinematics," in *Robotics, Vision and Control: Fundamental Algorithms in MATLAB®*, P. Corke, W. Jachimczyk, and R. Pillat Eds. Cham: Springer International Publishing, 2023, pp. 275-328.
[60] P. I. Corke, "A Simple and Systematic Approach to Assigning Denavit–Hartenberg Parameters," *IEEE Transactions on Robotics*, vol. 23, no. 3, pp. 590-594, 2007, doi: 10.1109/TRO.2007.896765.
[61] J. Denavit and R. S. Hartenberg, "A kinematic notation for lower-pair mechanisms based on matrices," 1955.
[62] K. M. Lynch and F. C. Park, *Modern robotics*. Cambridge University Press, 2017.
[63] M. Al-Fetyani, "plotworkspace - Plot workspace of n-DOF planar robot - File Exchange - MATLAB CentralFile Exchange - MATLAB Central," 2019/4/8 2023. Accessed: 2023/9/29. [Online]. Available: https://www.mathworks.com/matlabcentral/fileexchange/71136-plotworkspace-plot-workspace-of-n-dof-planar-robot?s_tid=mwa_osa_a
[64] U. o. W.-. Milwaukee, "Three striped moths (Family Geometridae)," 2015/2/10 2015. [Online]. Available: https://uwm.edu/field-station/three-striped-moths/.
[65] K. C. Allen, N. S. Little, and O. P. Perera, "Temporal Occurrence of Plusiinae on Soybean in the Mississippi River Delta," *Journal of Economic Entomology*, vol. 114, no. 2, pp. 723-727, 2021, doi: 10.1093/jee/toaa308.
[66] B. Siciliano, L. Sciavicco, L. Villani, and G. Oriolo, "Robotics. Advanced textbooks in control and signal processing," ed: Springer London, London, 2009.
[67] B. Jenett and K. Cheung, "Bill-e: Robotic platform for locomotion and manipulation of lightweight space structures," in *25th AIAA/AHS Adaptive Structures Conference*, 2017, p. 1876.
[68] E. Dertien and S. Stramigioli, "Basic maneuvers for an inspection robot for small diameter gas distribution mains," in *2011 IEEE International Conference on Robotics and Automation*, 9-13 May 2011 2011, pp. 3447-3448, doi: 10.1109/ICRA.2011.5980253.
[69] P. Corke, *Robotics and control: fundamental algorithms in MATLAB®*. springer Nature, 2021.
[70] L. Van Griethuijsen and B. Trimmer, "Locomotion in caterpillars," *Biological Reviews*, vol. 89, no. 3, pp. 656-670, 2014.
[71] J. Brackenbury, "Caterpillar kinematics," *Nature*, vol. 390, no. 6659, pp. 453-453, 1997/12/01 1997, doi: 10.1038/37253.
[72] J. Brackenbury, "Fast locomotion in caterpillars," *Journal of Insect Physiology*, vol. 45, no. 6, pp. 525-533, 1999/06/01/ 1999, doi: https://doi.org/10.1016/S0022-1910(98)00157-7.
[73] D. L. Wagner and A. C. Hoyt, "On Being a Caterpillar: Structure, Function, Ecology, and Behavior," in *Caterpillars in the Middle: Tritrophic Interactions in a Changing World*, R. J. Marquis and S. Koptur Eds. Cham: Springer International Publishing, 2022, pp. 11-62.